known to associate with the DGC, it is of interest to determine the level of syntrophins in the DGC fraction. We applied proteins from the DGC fraction and the homogenate to the gel so that amounts of dystrophin were the same. As shown in Figure 1B, syntrophin levels in the DGC fraction were 5 times less than that in the initial homogenate, whereas β-DG was present in similar amounts. Similar results were obtained using rabbit cardiac or skeletal muscles (data not shown). These results suggest that in muscle cells there exists a considerable amount of syntrophin which does not associate with the DGC. Although there is no direct evidence, we suppose the syntrophin in the soluble fraction to be derived from the cytosol or from complexes with other non-DGC proteins.

Syntrophin associates with actin and modulates its function

In order to determine whether the native syntrophin in the soluble fraction can associate with actin, we first partially purified syntrophin from rabbit cardiac muscles, as described in Materials and methods. Purified syntrophin from the soluble fraction (apparent molecular mass: 59 kDa) interacts with F-actin and calmodulin as revealed by actin co-sedimentation and calmodulin-Sepharose binding assays (data not shown), consistent with our previous findings (Iwata et al., 1998).

We next examined whether particular functions of actin are modulated by interaction with syntrophin. Addition of full-length recombinant syntrophin (M1–505) strongly inhibited actin-activated myosin ATPase activity (Fig. 2A), while recombinant MBP alone had no effect on actin-activated myosin ATPase activity (data not shown). Inhibition was almost complete at a 1:1 molar ratio of syntrophin to actin. Syntrophin also strongly inhibited the superprecipitation of actomyosin, which was monitored by measuring the increase in turbidity (Fig. 2B). Again, superprecipitation was almost completely inhibited at a 1:1 molar ratio of syntrophin to actin. These data suggest that interaction of actin with myosin is inhibited by syntrophin, presumably through competitive replacement by syntrophin.

Subcellular localization of syntrophin expressed in non-muscle and smooth muscle cells

We previously reported that PH2 and SU domains of syntrophin were required for interaction with F-actin (Iwata et al., 1998). To elucidate the role of actin-binding sites in subcellular localization of syntrophin, we first tried to confirm the actin-binding region of syntrophin by checking the interaction of newly-produced recombinant syntrophin proteins with F-actin. While deletion of both PH2 and SU domains abolished the interaction of syntrophin with F-actin, deletion of the SU domain alone preserved some ability for interaction (Fig. 3A). Furthermore, more precise analysis revealed that four regions of syntrophin, amino acids 274–291 (WVKDELQALLAAS-SPAGS), 317–328 (TEKELLLYGGLP), and 349–357 (VHSGPSKGS) in the PH2 domain and 497–505 (KVTRLGLLA) in the SU domain are important for interaction with actin (data not shown). Consistent with presence of multiple actin-binding sites, we observed that syntrophin induces the bundling of F-actin (data not shown).

We examined the subcellular localization of syntrophin by expressing exogenous syntrophin in CHO cells, which do not express detectable levels of endogenous syntrophin. As shown in Figure 3B, wild-type syntrophin was predominantly observed in the peripheral region of CHO cells. Cortical F-actin

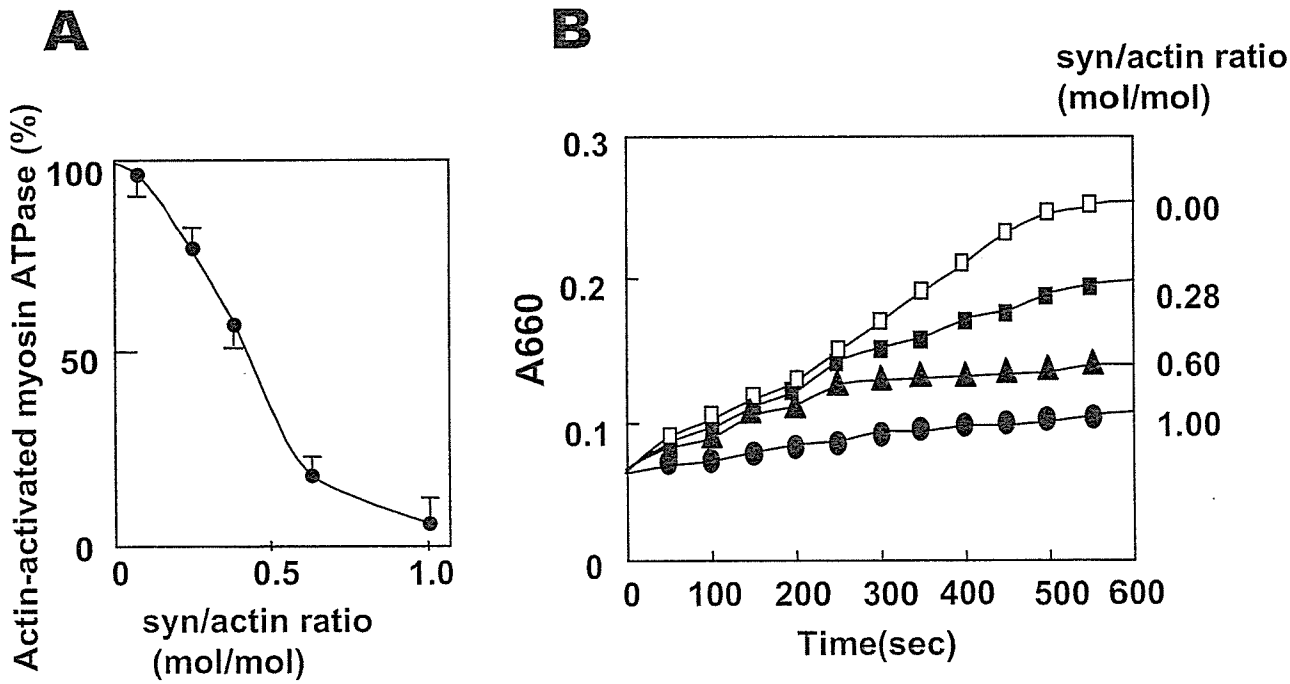

Fig. 2. Effect of syntrophin on actin-activated myosin ATPase activity and actomyosin superprecipitation. (A) The actin-activated myosin ATPase activity was measured in the presence of various concentrations of syntrophin, as described in Materials and methods. The ATPase activity for myosin alone (~0.04 μmol of Pi/mg/min), i.e., the activity without syntrophin, was subtracted for purposes of normalization. The data are shown as means ±S. D. of three determinations. (B) Time courses of changes in the turbidity were measured after mixing of actin and myosin in the presence of various concentrations of syntrophin.

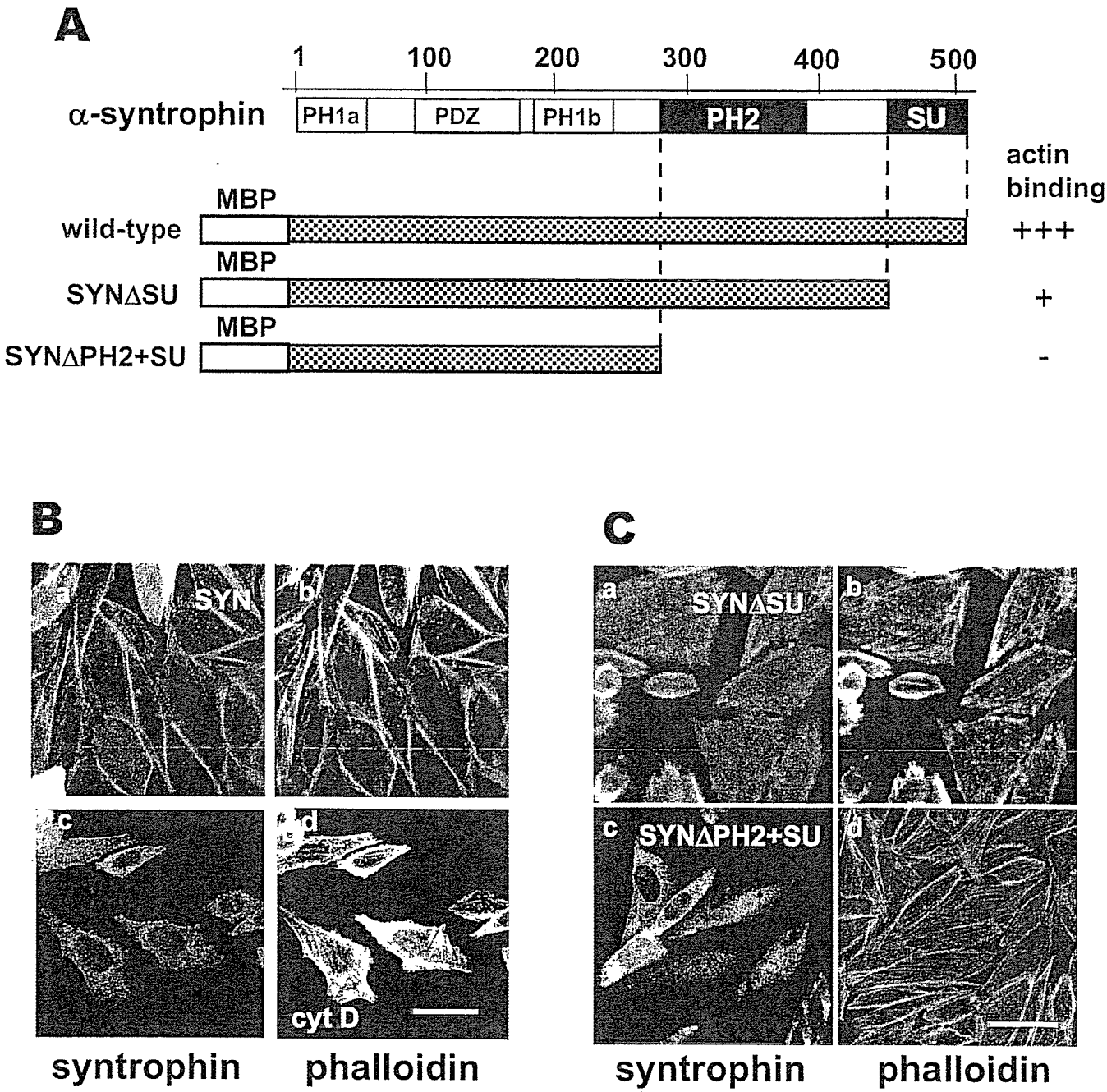

Fig. 3. Actin-binding ability and subcellular localization of the wild-type and deletion mutant syntrophins expressed in CHO cells. (A) Schematic representation of α-syntrophin and its deletion constructs. Recombinant full-length α-syntrophin and deletion mutants ΔSU (aa 449–505 deleted) and ΔPH2+SU (aa 274–505 deleted) fused with MBP were subjected to actin co-sedimentation assay. Actin-binding ability is indicated by +++, + and – for strong, weak and no interaction of syntrophin with actin, respectively. (B, C) Full-length syntrophin and deletion mutants (SYNΔSU and SYNΔPH2+SU) were expressed in CHO cells. Cells were immunostained with anti-pan-syntrophin antibody and FITC-conjugated secondary antibody (a and c) or with rhodamine-phalloidin (b and d). In (B, c and d), cells were treated for 15 min with 2 μM cytochalasin D. Bar 50 μm.

structures stained with rhodamine-phalloidin closely co-localized with syntrophin (Fig. 3B, b). Treatment with the actin-depolymerizing agent cytochalasin D disrupted the cortical actin structures and simultaneously abolished the peripheral localization of syntrophin, providing further evidence for the direct interaction of syntrophin with cortical F-actin. Figure 3C shows the results for mutant syntrophins lacking either the SU domain or both the SU and PH2 domains, which were shown above to be important for interaction with actin. Peripheral localization of syntrophin was markedly impaired upon deletion of the SU domain (SYNΔSU). However, it is noted that some mutant syntrophin (SYNΔSU) is still localized in the peripheral region. On the other hand, syntrophin almost completely disappeared from the peripheral region upon deletion of both the SU and PH2 domains (SYNΔPH2+SU), consistent with the finding that the SU and PH2 domains of

syntrophin are critical for actin binding. There was no apparent change in the peripheral localization of F-actin in the presence of the syntrophin deletion mutants (Fig. 3C).

We also examined syntrophin localization in bovine endothelial cells, which are known to have well-developed actin stress fibers. In this experiment, we transiently expressed GFP-tagged syntrophin in these cells and stained actin with rhodamine-phalloidin. The distribution of GFP-fluorescence coincided with that of rhodamine fluorescence (Fig. 4A), indicating that exogenous syntrophin co-localizes with actin fibers in endothelial cells. Moreover, endogenous syntrophin stained with anti-syntrophin antibody was also co-localized at

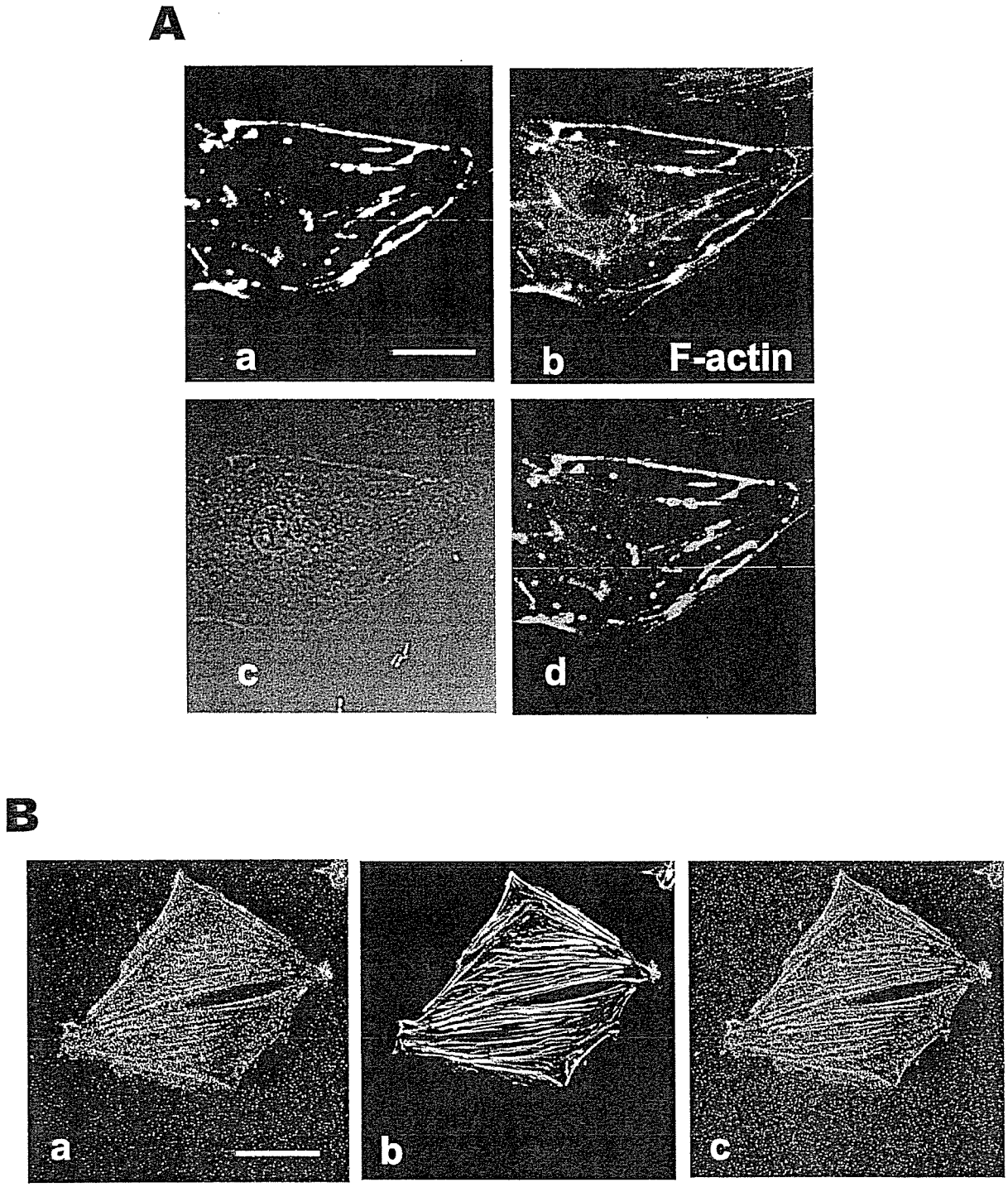

Fig. 4. Subcellular localization of syntrophin in endothelial cells and A7r5 smooth muscle cells. (**A**) GFP-tagged full-length syntrophin was expressed in bovine endothelial cells, fixed and stained with rhodamine-phalloidin. Images for GFP (a) and rhodamine fluorescence (b) and a corresponding phase-contrast image (c) are shown. A merged image is shown in (d). Original color information was omitted in (a and b). (B) A7r5 cells were co-stained with anti-syntrophin antibody (a) and phalloidin (b). A merged image is shown in c. Original color information was omitted in (a and b). Two cells are visible in these figures. Bars 35 μm (A), 50 μm (B).

least in part with stress fibers in aortic smooth muscle cell line A7r5 (Fig. 4B). This co-localization was also disrupted by treatment with cytochalasin D (data not shown).

Subcellular localization of syntrophin in skeletal muscle cells

We next examined subcellular localization of syntrophin in primary cultured skeletal myotubes. Syntrophin was predominantly localized in the peripheral membranes, but also slightly in the cytosol of skeletal myotubes (Fig. 5a). Consistent with the peripheral localization in primary cultured myotubes, most syntrophins were localized in the membranes in adult skeletal muscles (data not shown). Importantly, syntrophin did not appear to co-localize with actin in the contractile apparatus (Fig. 5a). Thus, syntrophin does not seem to interact with contractile actin despite its actin-binding ability. We assume that some syntrophin probably interacts with peripheral actin fibers which are not extensively stained with phalloidin in primary cultured myotubes. Despite being apparently not stained with phalloidin, cytoskeletal actin fibers were detected with antibodies against α-, β- and γ-actins (Rybakova et al., 2000).

Interestingly, when serum was removed, most syntrophins disappeared from the membrane region and became localized in the cytosol (Fig. 5d). Concomitantly, recovery of syntrophin into the soluble fraction significantly increased (data not shown). In addition, we observed that FCS or phorbol ester (PMA) stimulated translocation of syntrophin from the cytosol to the membrane in this primary cultured myotubes (data not shown). These data suggest that subcellular localization of syntrophin greatly depends on the physiological state of cells.

To further analyze the change in subcellular localization of syntrophin, we used C2C12 myotubes. Most endogenous syntrophin in serum-starved C2C12 myotubes appeared to be distributed in the cytosol (Fig. 6A, a). The staining pattern of syntrophin did not overlap with that of actin fibers probably corresponding to the myofibrils which are slightly present in C2C12 myotubes (Fig. 6A, a and b). This staining pattern of syntrophin was similar to that in the serum-starved primary myotubes (see Fig. 5d). Interestingly, treatment with LPA (10 μM) markedly increased the amount of syntrophin in the peripheral region of myotubes, with a concomitant increase in peripheral actin fibers (Fig. 6A, d and e). The change in syntrophin localization occurred 15 min after treatment with LPA (data not shown). Like LPA, the actin-stabilizing agent JAS also stimulated the translocation of syntrophin from the cytosol to the peripheral region (Fig. 6A, g). On the other hand, pretreatment with Lat B, which is known to destabilize actin fibers by sequestering G-actin monomers, blocked the LPA-induced translocation of syntrophin. In contrast to syntrophin, membrane localization of α-SG (Fig. 6A, c and f) and β-DG (data not shown) did not change upon stimulation with LPA. Translocation of syntrophin from the cytosol to the peripheral region was also confirmed by subcellular fractionation. By

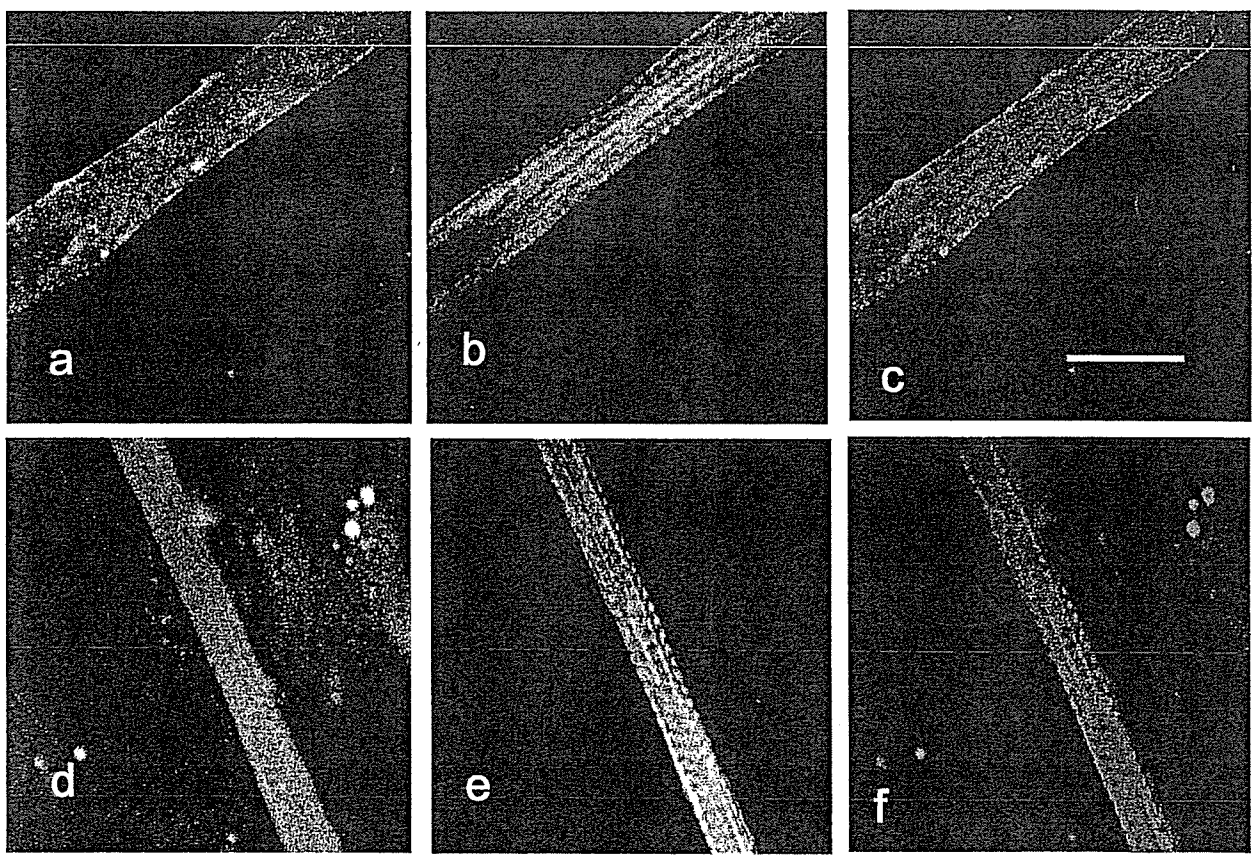

Fig. 5. Subcellular localization of endogenous syntrophin in cultured skeletal myotubes. Myotubes from hamster skeletal muscles were cultured under horse serum-supplemented (a–c) or serum-starved conditions overnight (d-f), and double-stained with anti-pan-syntrophin antibody (a, d) and rhodamine-phalloidin (b, e). A merged image is shown in (c and f). Original color information was omitted in (a, b, d and e). Bar 50 μm.

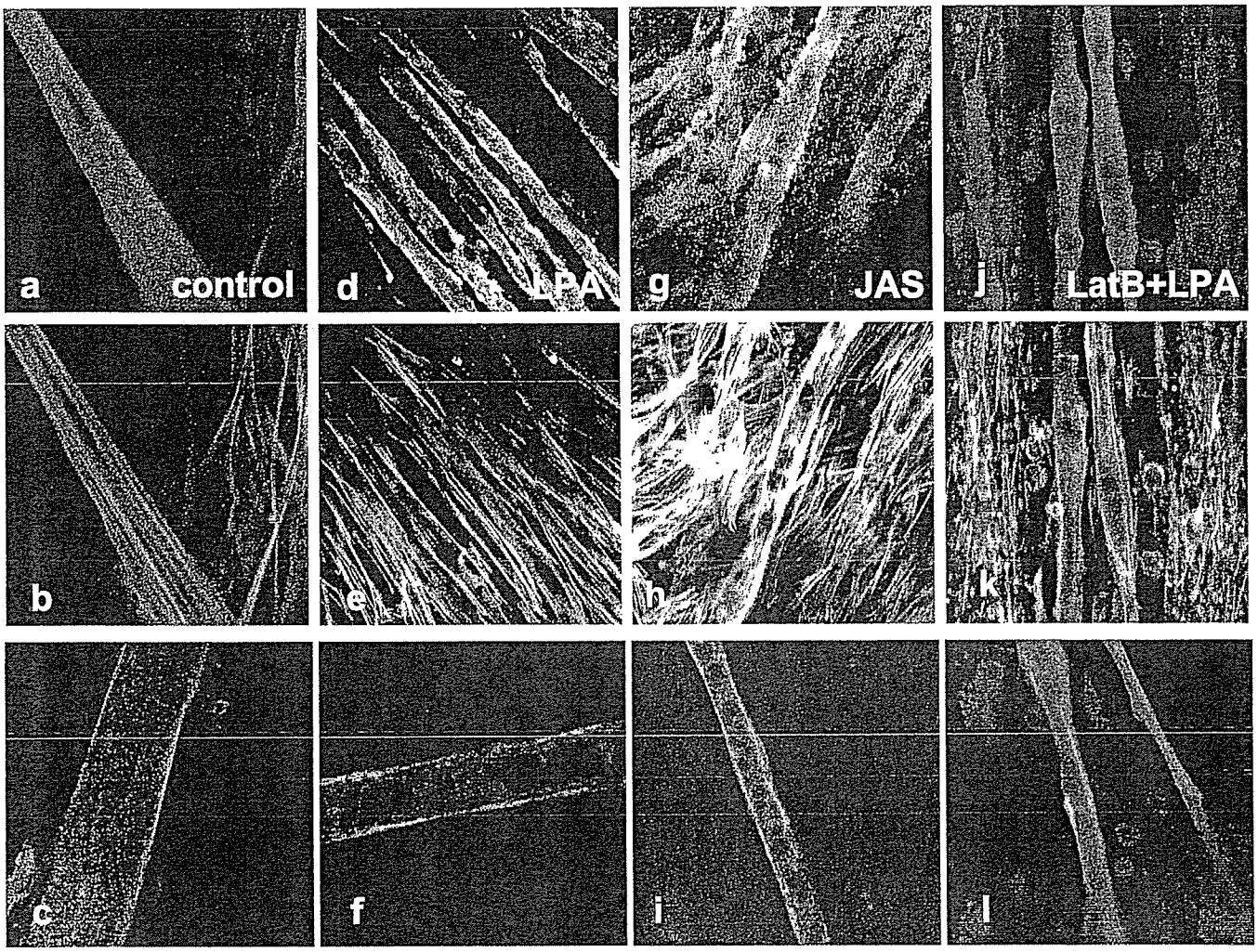
A
a control
d LPA
g JAS
j LatB+LPA
b
e
h
k
c
f
i
l

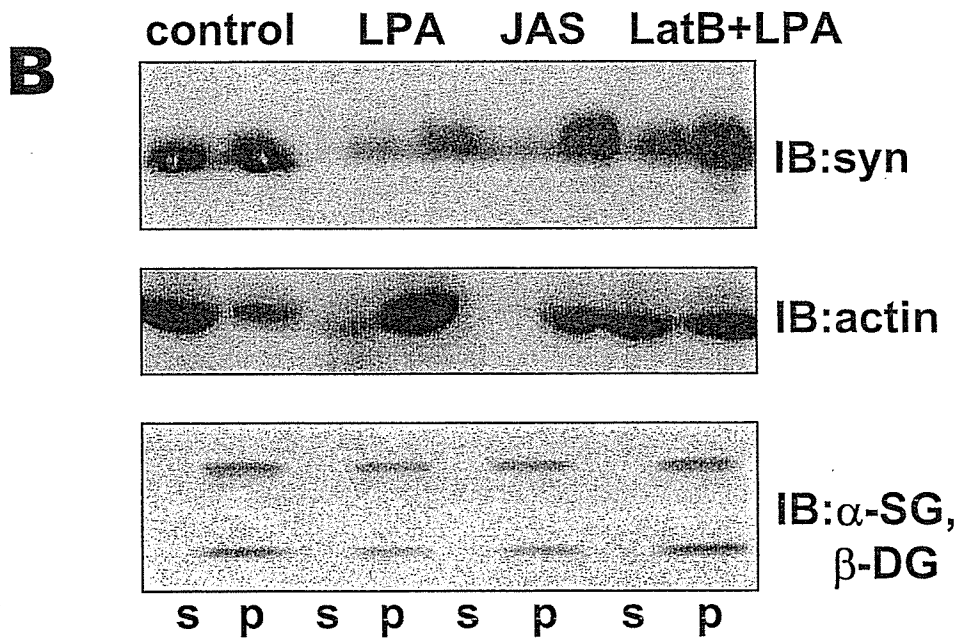
B
control LPA JAS LatB+LPA
IB:syn
IB:actin
IB:α-SG,
β-DG
s p s p s p s p

◀ **Fig. 6.** Effect of actin-perturbing agents on subcellular localization of syntrophin in C2C12 myotubes. (A) Subcellular localization of syntrophin. Mouse C2C12 myotubes were serum-depleted overnight. Cells were not treated (a–c) or treated for 20 min with 10 μM LPA (d–f), 1 h with 3 μM JAS (g–i) or pretreated for 15 min with 25 μM Lat B before LPA treatment (j–l). Cells were co-stained with anti-syntrophin antibody (a, d, g and j) and rhodamine-phalloidin (b, e, h and k). In (c, f, i and l), cells were stained with anti-α-SG antibody. (B) Subcellular fractionation after treatment with various agents. Cultured myotubes were homogenized for 30 s in 10 mM $NaHCO_3$ and after centrifugation the precipitated (P) and soluble (S) fractions were analyzed as described in Materials and methods.

high-speed centrifugation, we simply separated the cell homogenate into the soluble and the precipitate fractions. Upon addition of LPA or JAS, the amounts of syntrophin and actin in the cytosolic soluble fraction were relatively reduced as compared to those in the precipitate (Fig. 6B). Pretreatment with LatB suppressed these changes (Fig. 6B). These results suggest that localization of syntrophin in muscle cells may be regulated by extracellular signals through a cytoskeleton-dependent pathway.

Discussion

It has been widely postulated that syntrophin is a component of DGC, which mechanically stabilizes the sarcolemma by linking the cytoskeleton to the extracellular matrix. However, recent discoveries of various targets for syntrophin (for review see (Albrecht and Froehner, 2002)) have provided new insights into its function. In this study, we have characterized the biochemical properties of syntrophin, with a particular focus on syntrophin subcellular localization and interaction with F-actin.

Syntrophin as an actin-binding protein

We have previously reported that recombinant α-syntrophin binds to actin and calmodulin, based on results obtained using recombinant α-syntrophin (Iwata et al., 1998). In the current study, we have isolated native syntrophin from the cytosol of cardiac and skeletal muscle cells, and shown that similar to the recombinant syntrophin, native purified one has also the ability to bind F-actin and calmodulin. We also found that syntrophin inhibits actin-activated myosin ATPase activity and super-precipitation of actomyosin at a 1:1 syntrophin:actin molar ratio. These results suggest that syntrophin inhibits the interaction of actin and myosin by competitive interaction with actin filaments. Cofilin (Nishida et al., 1984), caldesmon and calponin (Shirinsky et al., 1992) have also been shown to inhibit actin-activated myosin ATPase activity and the interaction of caldesmon or calponin with actin filaments results in the inhibition of actin filament movement by smooth muscle myosin or by skeletal muscle heavy meromyosin (Shirinsky et al., 1992). Although further study is required, it is possible that syntrophin has also the ability to regulate muscle contraction by interacting with actin filaments in a similar manner to other actin-binding proteins under pathological conditions. However, such interaction of syntrophin with myofibrils does not appear to occur at least in normal skeletal myotubes (see Fig. 5). Rather, actin-binding ability of syntrophin appears to be related with other functions as discussed later.

We have identified four precise actin-binding regions within α1-syntrophin, of which three are in the PH2 domain and the fourth is in the SU domain (see Results). The three PH2 regions, amino acids 317–328 (TEKELLLYGGLP), 349–357 (VHSGPSKGS) and 497–505 (KVTRLGLLA), are well conserved among the α-, β1- and β2-isoforms (more than 70% amino acid identity). Consistent with the sequence conservation, we have also shown that β2-syntrophin binds to F-actin (unpublished data). The PH2 or SU domain of syntrophin is also known to interact with dystrophin family members, including dystrophin, utrophin and dystrobrevin (Kachinsky et al., 1999; Albrecht and Froehner, 2002). Thus, in cells it is possible that syntrophin localization alternates between actin filaments and the DGC.

We observed that α1-syntrophin expressed in CHO or endothelial cells co-localized with cortical peripheral F-actin and stress fibers, consistent with the in vitro binding study. This was reinforced by the finding that cytochalasin D, an actin-depolymerizing agent, simultaneously destroyed F-actin fibers and disrupted co-localization of syntrophin (Fig. 3B). While deletion of both the SU and PH2 domains almost completely abolished co-localization of syntrophin with actin fibers, the interaction of syntrophin with actin fibers in CHO cells was partly preserved upon deletion of the SU domain alone. Therefore, the PH2 domain appears to be critical for interaction of syntrophin with F-actin in living cells. Such a PH domain-mediated interaction with F-actin has also been reported for Bruton's tyrosine kinase (Yao et al., 1999).

Subcellular localization and translocation of syntrophin

We found that some syntrophin was present in the soluble fraction after subcellular fractionation of cardiac and skeletal muscle tissues, and that the native syntrophin from the soluble fraction is capable of binding both actin and calmodulin. In cultured myotubes under serum-depleted conditions, endogenous syntrophins were predominantly localized in the cytosol (Figs. 5d and 6A), in sharp contrast to syntrophins expressed in CHO and endothelial cells or endogenous syntrophin in A7r5 smooth muscle cells. Interestingly, LPA induced translocation of syntrophin from the cytosol to the peripheral region, with a concomitant increase in actin fibers. In addition, syntrophin translocation was stimulated by JAS and inhibited by LatB (Fig. 6A), suggesting that actin fiber formation is required for translocation. Together, these findings suggest that a part of α-syntrophin is not present as a static complex with DGC, but that its localization is dynamically regulated via cytoskeletal reorganization in skeletal muscle cells.

LPA is known to induce actin cytoskeleton organization via Rho GTPase kinase activation (Niu et al., 2003). LPA is also known to activate protein kinase C and proline-rich tyrosine kinase 2 (Pyk2) (Wu et al., 2002), similarly to other G protein-coupled receptor agonists. We found that α-syntrophin is phosphorylated by PKC (unpublished results), and that a PKC activator, phorbol ester stimulates translocation of α-syntrophin to the membrane (see Results). Other studies have indicated that α1-syntrophin is also phosphorylated by stress-activated protein kinase (Hasegawa et al., 1999), or by certain serine/threonine kinases (Lumeng et al., 1999). Therefore, it is likely that a phosphorylation-dependent mechanism may be involved in LPA-induced syntrophin translocation, but the

precise mechanism remains to be determined. Following this line of thought, it is of interest to note that phosphorylation/dephosphorylation regulates the interaction of myristoylated alanine-rich C-kinase substrate (MARCKS) with actin fibers (Hartwig et al., 1992). The interaction of MARCKS with actin fibers occurs only when it is dephosphorylated, and PKC-induced phosphorylation has been shown to displace MARCKS from the plasma membrane to the cytosol (Hartwig et al., 1992).

In adult skeletal muscle tissues, α-syntrophin is mainly localized in the peripheral regions and at neuromuscular junctions (Peters et al., 1997). However, we found that a considerable amount of syntrophin was recovered in the soluble fraction from skeletal muscles, in which the DGC is not present. Therefore, it is likely that part of syntrophin associates with non-DGC proteins in the peripheral regions and is thereby recovered in the soluble fraction after homogenization in the hypotonic buffer, although we do not exclude the possibility that part of syntrophin exists in the cytosol. In fact, syntrophin was present both in the plasma membrane and the cytosol in primary cultured myotubes. The peripheral localization of α-syntrophin in native muscle or primary myotubes is in contrast to observations in non-stimulated C2C12 or serum-starved myotubes. This discrepancy may be due to the difference in the extent of muscle differentiation or in some physiological states of myotubes. For example, skeletal muscles are innervated, while the myotubes are not. In skeletal muscles, innervations induce the clustering of acetylcholine receptors (AchR), and recently AchR clustering has been shown to be induced by extracellular matrix proteins such as agrin and laminin (Moransard et al., 2003). However, in normal differentiation medium, C2C12 myotubes do not have well-developed AchR clusters at the basement membrane, although the extent of cell differentiation is dependent on the composition of the culture medium (Portier et al., 1999). Thus, our present findings raise the interesting possibility that in early muscle cells or serum-starved myotubes, α-syntrophin may localize mostly in the cytosol, thereby sequestering various soluble proteins such as calmodulin and serine/threonine kinases, and then recruit these signaling molecules to the membrane during muscle maturation or muscle stimulation. Consistent with this idea, we recently observed that laminin-1 induces syntrophin translocation from the cytosol to the membrane in C2C12 myotubes (Iwata, unpublished observation).

Physiological and pathological implications

Dystrophin was the first disease-relevant protein shown to be enriched at costameres, where syntrophins and cytoskeletal γ-actin also co-exist. Although dystrophin and syntrophin are not required for the assembly of costameres, their absence in humans and mice leads to a disorganized costameric lattice and disruption of sarcolemmal integrity (for review see (Ervasti, 2003)). A syntrophin-actin interaction would contribute to strengthening the mechanical coupling between the sarcolemma and actin filaments in costameres during muscle contraction. Although mice lacking α-syntrophin do not have a dystrophic phenotype (Kameya et al., 1999), the postsynaptic membrane is grossly abnormal and the amount of acetylcholine receptors (AchR and AchE) is significantly decreased (Adams et al., 2000). Another recent report shows that actin polymerization induced by synaptogenic signals is necessary for the movement and formation of AchR clusters (Dai et al., 2000). On the other hand, γ2-syntrophin has been reported to regulate the gating of the cardiac and intestinal smooth muscle mechanosensitive Na^+ channel SCN5A through a PDZ domain-mediated interaction (Ou et al., 2003). Hence, it is plausible that dynamic regulation of syntrophins by actin plays an important role in many physiological or pathological processes.

Acknowledgements. We thank Drs. Hirofumi Onishi and Takashi Ohki for a generous gift of skeletal actin. We thank Dr. Stanley C. Froehner for a gift of SYN1351. This work was supported by Grant-in-Aid 14580664 and 14570708, and Grant-in-Aid for Priority Areas 13142210 from the Ministry of Education, Culture, Sports, Science and Technology of Japan and by a grant for Promotion of Fundamental Studies in Health Science from the Organization of Pharmaceutical Safety and Research.

References

Adams, M. E., Kramarcy, N., Krall, S. P., Rossi, S. G., Rotundo, R. L., Sealock, R., Froehner, S. C., 2000. Absence of α-syntrophin leads to structurally aberrant neuromuscular synapses deficient in utrophin. J. Cell Biol. 150, 1385–1397.

Ahn, A. H., Freener, C. A., Gussoni, E., Yoshida, M., Ozawa, E., Kunkel, L. M., 1996. The three human syntrophin genes are expressed in diverse tissues, have distinct chromosomal locations, and each bind to dystrophin and its relatives. J. Biol. Chem. 271, 2724–2730.

Albrecht, D. E., Froehner, S. C., 2002. Syntrophins and dystrobrevins: defining the dystrophin scaffold at synapses. Neurosignals 11, 123–129.

Amiry-Moghaddam, M., Williamson, A., Palomba, M., Eid, T., de Lanerolle, N. C., Nagelhus, E. A., Adams, M. E., Froehner, S. C., Agre, P., Ottersen O. P., 2003. Delayed K^+ clearance associated with aquaporin-4 mislocalization: Phenotypic defects in brains of α-syntrophin-null mice. Proc. Natl. Acad. Sci. USA 100, 13615–13620.

Brenman, J. E., Chao, D. S., Gee, S. H., McGee, A. W., Craven, S. E., Santillano, D. R., Wu, Z., Huang, F., Xia, H., Peters, M. F., Froehner, S. C., Bredt, D. S., 1996. Interaction of nitric oxide synthase with the postsynaptic density protein PSD-95 and α1-syntrophin mediated by PDZ domains. Cell 84, 757–767.

Campbell, K. P., 1995. Three muscular dystrophies: Loss of cytoskeleton-extracellular matrix linkage. Cell 80, 675–679.

Chockalingam, P. S., Gee, S. H., Jarrett, H. W., 1999. Pleckstrin homology domain 1 of mouse α1-syntrophin binds phosphatidylinositol 4,5-bisphosphate. Biochemistry 38, 5596–5602.

Dai, Z., Luo, X., Xie, H., Peng, H. B., 2000. The actin-driven movement and formation of acetylcholine receptor clusters. J. Cell Biol. 150, 1321–1334.

Ervasti, J. M., 2003. Costameres: the Achilles' Heel of Herculean muscle. J. Biol. Chem. 278, 13591–13594.

Gee, S. H., Madhavan, R., Levinson, S. R., Caldwell, J. H., Sealock, R., Froehner, S. C., 1998. Interaction of muscle and brain sodium channels with multiple members of the syntrophin family of dystrophin-associated proteins. J. Neurosci. 274, 128–137.

Hartwig, J. H., Thelen, M., Rosen, A., Janmey, P. A., Nairn, A. C., Aderem, A., 1992. MARCKS is an actin filament crosslinking protein regulated by protein kinase C and calcium-calmodulin. Nature 356, 618–622.

Hasegawa, M., Cuenda, A., Spillantini, M. G., Thomas, G. M., Buee-Scherrer, V., Cohen, P., Goedert, M., 1999. Stress-activated protein kinase-3 interacts with the PDZ domain of α1-syntrophin. J. Biol. Chem. 274, 12626–12631.

Hosaka, Y., Yokota, T., Miyagoe-Suzuki, Y., Yuasa, K., Imamura, M., Matsuda, R., Ikemoto, T., Kameya, S., Takeda, S., 2002. alpha1-Syntrophin-deficient skeletal muscle exhibits hypertrophy and aberrant formation of neuromuscular junctions during regeneration. J. Cell Biol. 158, 1097–1107.

Iwata, Y., Pan, Y., Hanada, H., Yoshida, T., Shigekawa, M., 1996. Dystrophin-glycoprotein complex purified from hamster cardiac muscle. Comparison of the complexes from cardiac and skeletal muscles of hamster and rabbit. J. Mol. Cell. Cardiol. 28, 2501–2509.

Iwata, Y., Pan, Y., Yoshida, T., Hanada, H., Shigekawa, M., 1998. α1-Syntrophin has distinct binding sites for actin and calmodulin. FEBS Lett. 423, 173–177.

Kachinsky, A. M., Froehner, S. C., Milgram, S. L., 1999. A PDZ-containing scaffold related to the dystrophin complex at the basolateral membrane of epithelial cells. J. Cell Biol. 145, 391–402.

Kameya, S., Miyagoe, Y., Nonaka, I., Ikemoto, T., Endo, M., Hanaoka, K., Nabeshima, Y.-I., Takeda, S., 1999. α1-syntrophin gene disruption results in the absence of neuronal-type nitric-oxide synthase at the sarcolemma but does not induce muscle degeneration. J. Biol. Chem. 274, 2193–2200.

Lumeng, C., Phelps, S., Crawford, G. E., Walden, P. D., Barald, K., Chamberlain, J. S., 1999. Interactions between β2-syntrophin and a family of microtubule-associated serine/threonine kinases. Nat. Neurosci. 2, 611–617.

Moransard, M., Borges, L. S., Willmann, R., Marangi, P. A., Brenner, H. R., Ferns, M. J., Fuhrer, C., 2003. Agrin regulates rapsyn interaction with surface acetylcholine receptors, and this underlies cytoskeletal anchoring and clustering. J. Biol. Chem. 278, 7350–7359.

Nishida, E., Maekawa, S., Sakai, H., 1984. Cofilin, a protein in porcine brain that binds to actin filaments and inhibits their interactions with myosin and tropomyosin. Biochemistry 23, 5307–5313.

Niu, J., Profirovic, J., Pan, H., Vaiskunaite, R., Voyno-Yasenetskaya, T., 2003. G protein βγ subunits stimulate p114RhoGEF, a guanine nucleotide exchange factor for RhoA and Rac1: regulation of cell shape and reactive oxygen species production. Circ. Res. 93, 848–856.

Ou, Y., Strege, P., Miller, S. M., Makielski, J., Ackerman, M., Gibbons, S. J., Farrugia, G., 2003. Syntrophin γ2 regulates SCN5A gating by a PDZ domain-mediated interaction. J. Biol. Chem. 278, 1915–1923.

Ozawa, E., Noguchi, S., Mizuno, Y., Hagiwara, Y., Yoshida, M., 1998. From dystrophinopathy to sarcoglycanopathy: evolution of a concept of muscular dystrophy. Muscle Nerve 21, 421–438.

Perry, S. V., 1955. Myosin adenosinetriphosphatase. Methods Enzymol. 2, 582–588.

Peters, M. F., Adams, M. E., Froehner, S. C., 1997. Differential association of syntrophin pairs with the dystrophin complex. J. Cell Biol. 138, 81–93.

Piluso, G., Mirabella, M., Ricci, E., Belsito, A., Abbondanza, C., Servidei, S., Puca, A. A., Tonali, P., Puca, G. A., Nigro, V., 2000. γ1- and γ2-Syntrophins, two novel dystrophin-binding proteins localized in neuronal cells. J. Biol. Chem. 275, 15851–15860.

Portier, G. L., Benders, A. G., Oosterhof, A., Veerkamp, J. H., van Kuppevelt, T. H., 1999. Differentiation markers of mouse C2C12 and rat L6 myogenic cell lines and the effect of the differentiation medium. In Vitro Cell Dev. Biol. Anim. 35, 219–227.

Rybakova, I. N., Amann, K. J., Ervasti J. M., 1996. A new model for the interaction of dystrophin with F-actin. J. Cell Biol. 135, 661–672.

Rybakova, I. N., Jitandrakumar R. P., Ervasti J. M., 2000. The dystrophin complex forms a mechanically strong link between the sarcolemma and costameric actin. J. Cell Biol. 150, 1209–1214.

Sampaolesi, M., Yoshida T., Iwata Y., Hanada, H., Shigekawa M., 2001. Stretch-induced cell damage in sarcoglycan-deficient myotubes. Pflügers Arch. 442, 161–170.

Shirinsky, V. P., Biryukov, K. G., Hettasch, J. M. Seller, J. R., 1992. Inhibition of the relative movement of actin and myosin by caldesmon and calponin. J. Biol. Chem. 267, 15886–15892.

Spudich, J., Watt, S., 1974. The regulation of rabbit skeletal muscle contraction. J. Biol. Chem. 216, 1866–1871.

Straub, V., Campbell, K. P., 1997. Muscular dystrophies and the dystrophin-glycoprotein complex. Curr. Opin. Neurol. 10, 168–175.

Tawada-Iwata, Y., Imagawa, T., Yoshida, A., Takahashi, M., Nakamura, H., Shigekawa, M., 1993. Increased mechanical extraction of T-tubule/junctional SR from cardiomyopathic hamster heart. Am. J. Physiol. 264, H1447-H1453.

Tinsley, J. M., Blake, D. J., Zuellig, R. A., Davies, K. E., 1994. Increasing complexity of the dystrophin-associated protein complex. Proc. Natl. Acad. Sci. USA 91, 8307–8313.

Towbin, J. A., Bawles, N. E., 2002. The failing heart. Nature 415, 227–233.

van Veldhoven, P. P., Mannaerts, G. P., 1987. Inorganic and organic phosphate measurements in the nanomolar range. Anal. Biochem. 161, 45–48.

Wu, S. S., Chiu, T., Rozengurt, E., 2002. ANG II and LPA induce Pyk2 tyrosine phosphorylation in intestinal epithelial cells: role of Ca^{2+}, PKC, and Rho kinase. Am. J. Physiol. Cell. Physiol. 282, C1432-C1444.

Yao, L., Janmey, P., Frigeri, L. G., Han, W., Fujita, J., Kawakami, Y., Apgar, J. R., Kawakami, T., 1999. Pleckstrin homology domains interact with filamentous actin. J. Biol. Chem. 274, 19752–19761.

Yoshida, T., Pan, Y., Hanada, H., Iwata, Y., Shigekawa, M., 1998. Bidirectional signaling between sarcoglycans and the integrin adhesion system in cultured L6 myocytes. J. Biol. Chem. 273, 1583–1590.

Characterisation of [^{123}I]iomazenil distribution in a rat model of focal cerebral ischaemia in relation to histopathological findings

Tomohito Kaji[1], Yuji Kuge[2], Chiaki Yokota[3], Masafumi Tagaya[5], Hiroyasu Inoue[4], Tohru Shiga[1], Kazuo Minematsu[6], Nagara Tamaki[1]

[1] Department of Nuclear Medicine, Hokkaido University Graduate School of Medicine, Kita-ku, Sapporo, Japan
[2] Department of Tracer Kinetics, Hokkaido University Graduate School of Medicine, Kita-ku, Sapporo, Japan
[3] Department of Pathogenesis, Research Institute, National Cardiovascular Center, Suita, Osaka, Japan
[4] Department of Pharmacology, Research Institute, National Cardiovascular Center, Suita, Osaka, Japan
[5] Department of Internal Medicine, National Osaka Hospital, Chuo-ku, Osaka, Japan
[6] Cerebrovascular Division, Department of Medicine, National Cardiovascular Center, Suita, Osaka, Japan

Received: 14 May 2003 / Accepted: 27 July 2003 / Published online: 8 October 2003

Abstract. Iodine-123 labelled iomazenil ([^{123}I]IMZ) has been reported to be a useful marker of neuronal viability. The brain distribution of [^{123}I]IMZ, however, has not been correlated with the pathophysiological response in detail after an ischaemic insult. To characterise [^{123}I]IMZ as a marker of neuronal viability, we compared its brain distribution with cyclooxygenase-2 (COX-2) expression, DNA fragmentation and cellular integrity. [^{123}I]IMZ and [^{125}I]IMP were injected into rats with focal cerebral ischaemia for the purpose of dual-tracer autoradiography. COX-2 and microtubule-associated protein-2 (MAP-2, a marker of cellular integrity) were immunostained. In situ DNA polymerase-I-dependent dUTP incorporation into damaged DNA was used as an indicator of DNA fragmentation. Lesion to normal ratios (LNRs) for [^{123}I]IMP and [^{125}I]IMZ were calculated. [^{123}I]IMZ accumulation was preserved in several regions with impaired [^{123}I]IMP accumulation. COX-2 expression was occasionally observed, whereas neither DNA fragmentation nor MAP-2 denaturation was detected in these regions. DNA fragmentation and impaired MAP-2 immunostaining were observed only in the regions with reduced LNRs for both tracers. The LNR for [^{123}I]IMZ was significantly lower in regions with impaired MAP-2 immunostaining (0.120±0.152, $P<0.0001$), in regions positive for dUTP incorporation (0.488±0.166, $P<0.0001$) and in regions positive for COX-2 expression (0.626±0.186, $P<0.001$) than in histologically normal regions (0.784±0.213). Thus, neuronal DNA is still intact and cellular integrity is maintained in the ischaemic regions with preserved [^{123}I]IMZ accumulation. The impairment of [^{123}I]IMZ accumulation precedes DNA fragmentation and denaturation of cellular integrity. These results provide the molecular basis of [^{123}I]IMZ distribution.

Keywords: [^{123}I]iomazenil – Cerebral ischaemia – Neuronal viability – Cyclooxygenase-2 – DNA fragmentation

Eur J Nucl Med Mol Imaging (2004) 31:64–70
DOI 10.1007/s00259-003-1319-6

Nagara Tamaki (✉)
Department of Nuclear Medicine,
Hokkaido University Graduate School of Medicine,
Kita 15 Nishi 7, 060-8638 Kita-ku, Sapporo, Japan
e-mail: natamaki@med.hokudai.ac.jp
Tel.: +81-11-7065150, Fax: +81-11-7067155

Introduction

An ischaemic stroke is one of the most common neuronal disorders, and the number of patients suffering from the disease is increasing. For the clinical evaluation of ischaemic stroke, it is very important to precisely detect the ischaemic penumbra, which is an ischaemically affected but still viable tissue, because the penumbral tissue can be salvaged by pharmacological and/or surgical interventions [1, 2, 3, 4].

Iodine-123 iomazenil ([^{123}I]IMZ) is a probe for central-type benzodiazepine receptor (BZR) for single-photon emission tomography (SPET). Since GABA receptors are abundant in the cortex and sensitive to ischaemic damage, specific radioligands to their subunits, the cerebral BZRs existing in GABA-A receptors, can be used as a marker of neuronal viability [5]. Thus, BZR imaging with [^{123}I]IMZ should be useful for detecting viable neurons, which may help detect the penumbra after an isch-

aemic insult. In this regard, several experimental and clinical investigators have compared the [^{123}I]IMZ distribution with the cerebral blood flow, oxygen metabolism and/or glucose metabolism, and shown the potential of [^{123}I]IMZ for evaluation of neuronal viability after an ischaemic stroke [3, 6, 7, 8, 9, 10, 11, 12]. A few authors [6, 10, 11] have also correlated [^{123}I]IMZ distribution with histological findings obtained using the haematoxylin-eosin stain.

To the best of our knowledge, however, the brain distribution of [^{123}I]IMZ has not been correlated with the molecular response after an ischaemic insult in detail. The pathophysiological significance of findings that are actually imaged by [^{123}I]IMZ also remains to be elucidated. Accordingly, we compared the brain distribution of [^{123}I]IMZ with (1) cerebral blood flow, (2) the expression of cyclooxygenase-2 (COX-2), (3) fragmentation of DNA and (4) cellular integrity, in order to characterise [^{123}I]IMZ as a marker of neuronal viability. COX-2, a prostanoid synthesising enzyme, is expressed early after an ischaemic insult and contributes to the progression of ischaemic damage [13, 14, 15, 16, 17]. Thus, we examined COX-2 expression to evaluate the neuronal response early after an ischaemic insult. In situ DNA polymerase-I-dependent dUTP incorporation into damaged DNA was used as an indicator of DNA fragmentation. Techniques for visual detection and localisation of DNA injury/repair in situ include: TdT-dependent dUTP labelling of free 3'-OH ends of double-stranded DNA (TUNEL); Klenow fragment of DNA polymerase-I-dependent labelling of staggered 3'-OH ends and gaps; and DNA polymerase-I incorporation in nicks, gaps and staggered 3'-OH ends [18]. Of these, only DNA polymerase-I has 5'–>3' exonucleolytic activity, which allows nick translation and visualisation of randomly occurring single-strand scission of double-stranded DNA. MAP-2, a cellular structural protein existing on the surface of neurodendrites, is also immunostained as a marker of cellular integrity.

Materials and methods

Animal preparation. The experimental protocol was fully approved by the Laboratory Animal Care and Use Committee of Hokkaido University. Male Sprague-Dawley rats weighing 300–350 g were used. The rats had free access to water and laboratory chow. The animals were initially anaesthetised with 400 mg/kg body weight IP chloral hydrate. The body temperatures were monitored with rectal probes and maintained at 37°C with heating pads during the operation. The rats were subjected to permanent unilateral major artery occlusion. The right middle cerebral artery (MCA) of each rat was occluded intraluminally according to a method described in detail previously [19, 20, 21]. The rats were allowed to recover from anaesthesia and any induced neurological deficits were confirmed. The animals not showing any neurological deficits were excluded from this experiment.

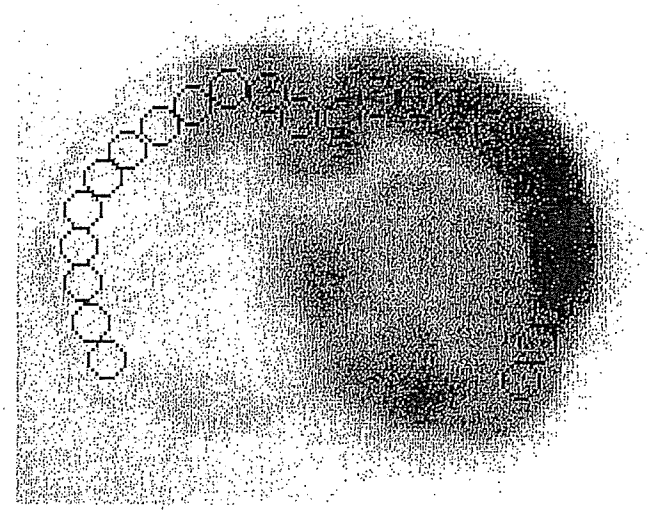

Fig. 1. An example of regions of interest (ROIs) on a coronal image. Twelve circular ROIs (2 mm in diameter) were determined on each hemisphere of the cortex symmetrically

Autoradiographic studies. The brain distributions of [^{123}I]IMZ and [^{125}I]IMP were determined using a dual-tracer autoradiographic technique. [^{123}I]IMZ (111 MBq/kg body weight) was first injected via the femoral vein 60 min before decapitation, to determine specific [^{123}I]IMZ distribution according to the methods reported by Toyama et al. [10, 11]. Then, 55 min later, [^{125}I]IMP (2.22 MBq/kg body weight) was injected via the contralateral femoral vein, to assess blood flow distribution [10, 11]. The rats were decapitated under chloral hydrate anaesthesia 5 min after the injection of [^{125}I]IMP, which was 2, 3, 4, 6, 8, 12 and 24 h after the ischaemic insult (n = four to six in each group). Their brains were removed quickly and carefully, and immersed in ice-cold saline. The brains were then sectioned at 6 mm caudal from the frontal pole using a brain matrix (RBM-4000C, ASI Instruments, Warren, MI) to obtain coronal sections. The brain samples were embedded in a medium (Tissue-Tek, Sakura Finetechnical Co., Ltd., Tokyo, Japan), frozen in isopentane-dry ice, and cut into 20-μm sections with a cryostat (Bright Instrument Co., Ltd., Cambridgeshire, England). The first autoradiographic exposure was performed for 3 h to detect the distribution of [^{123}I]IMZ. The second exposure was initiated 7 days later and carried out for 7 days to visualise the distribution of [^{125}I]IMP.

Histological studies. Immunoreactivity to COX-2 and microtubule-associated protein-2 (MAP-2) were detected in frozen sections (10 μm thick) adjacent to those used for the autoradiographic studies, using a standard immunostaining procedure [23]. Briefly, after fixation in a cold 1:1 acetone-to-methanol mixture, the sections were incubated with a polyclonal anti-COX-2 antibody (Cayman Chemical; dilution 1:2,000) or a purified mouse monoclonal anti-MAP-2 antibody (BD Pharmingen, San Diego; dilution 1:400). The bound antibody was visualised by staining with avidin/biotin conjugate immunoperoxidase (Vector Laboratories, Inc., CA, USA) and 3,3'-diaminobenzidine tetrahydrochloride (DAB; Vectastain Elite Kit, Vector Laboratories, CA).

DNA fragmentation was also detected on the adjacent sections by incorporation of digoxigenin-dUTP using DNA polymerase-I according to the method previously described [18, 23]. To confirm the nuclear localisation of the label, some sections were counterstained with haematoxylin.

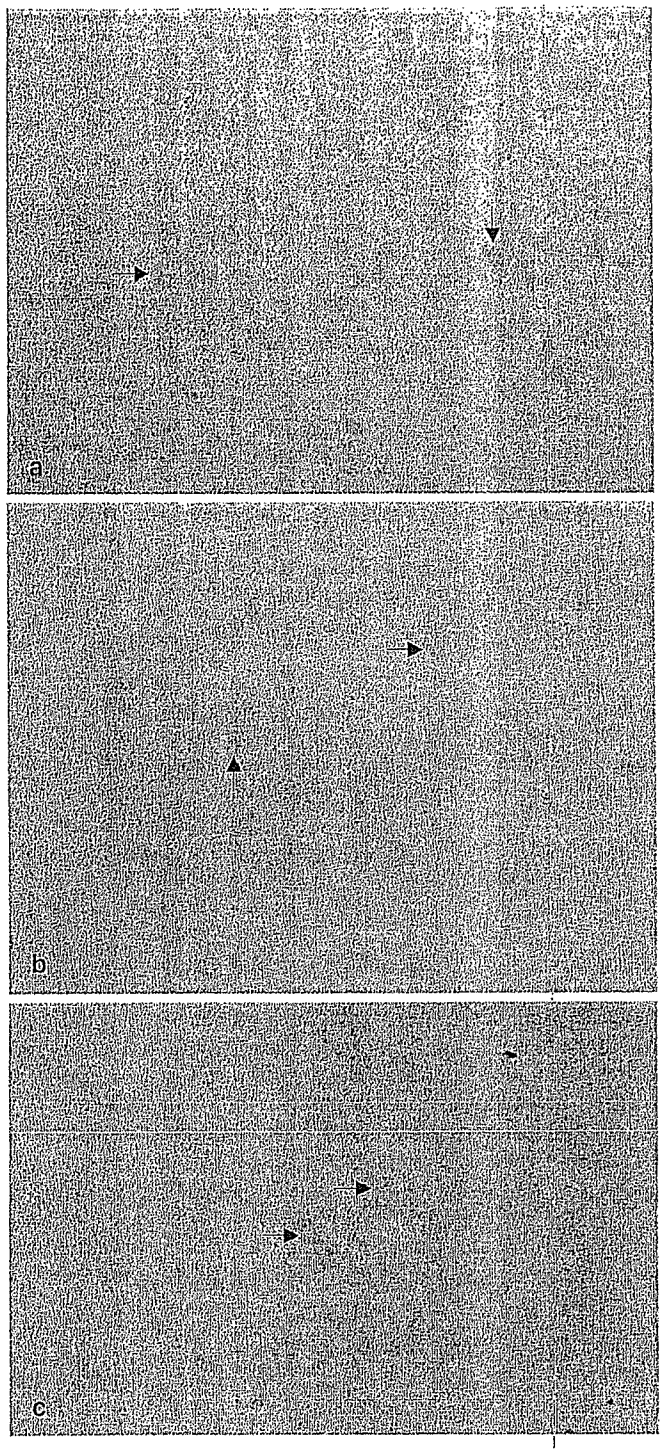

Data analysis. The autoradiograms were analysed using a computerised imaging analysis system (Bio-imaging Analyser BAS-5000, Fuji Photo Film, Tokyo, Japan). To quantitatively evaluate the distributions of [^{123}I]IMZ and [^{125}I]IMP, 12 circular regions of interest (ROIs, 2 mm in diameter) were determined on each hemisphere of the cerebral cortex in the autoradiograms symmetrically from the longitudinal fissure to the temporal lobe (Fig. 1). Lesion to normal ratios (LNRs) were defined as the ratios of values for an ROI in the lesioned hemisphere to those for the contralateral homologous ROI.

Based on the LNRs for [^{123}I]IMZ and [^{125}I]IMP, ROIs determined on the lesioned hemisphere were classified into three groups as shown in Table 1: group 1, LNRs for both [^{125}I]IMP and [^{123}I]IMZ were equal to or larger than 0.8; group 2, the LNRs for [^{125}I]IMP were less than 0.8 and those for [^{123}I]IMZ were equal to or larger than 0.8; group 3, LNRs for both [^{125}I]IMP and [^{123}I]IMZ were less than 0.8. A threshold LNR of 0.8 was chosen, considering the lesion detectability by the autoradiographic methods [11].

The ROIs determined on the lesioned hemisphere were also classified into four groups based on histological findings as follows (Fig. 2): group A, impaired MAP-2 immunostaining; group B, preserved MAP-2 immunostaining and positive for dUTP incorporation; group C, preserved MAP-2 immunostaining, negative for dUTP incorporation and positive for COX-2; group D, no histological evidence of an ischaemic injury.

All values are expressed as means or means ± standard deviation. A Z test was used to assess the significance of difference in the percentage of ROIs with impaired [^{125}I]IMP or [^{123}I]IMZ accumulation. One-way ANOVA and post-hoc tests (Fisher's method) were used to assess the significance of difference in the LNRs among the four groups classified on the basis of histological findings. A two-tail value of $P<0.05$ was considered to indicate statistical significance.

Results

Figure 3 shows representative autoradiograms for [^{125}I]IMP and [^{123}I]IMZ. The accumulation of [^{125}I]IMP decreased in a wide region in the MCA territory 2 h after occlusion, which extended with time. The region with

Fig. 2a–c. Representative images of a COX-2 immunostaining (×200), b dUTP incorporation (×200) and c MAP-2 immunostaining (×200). a Expression of COX-2 protein was occasionally observed (*arrows*). b The ring-like appearance (*arrows*) of dUTP incorporation shows the neuron on the way to apoptotic cell death. c Positive MAP-2 immunostaining (*arrows*) shows cellular integrity

Table 1. Histological findings in the three ROI groups classified on the basis of LNRs

Group	LNR_{IMP}	LNR_{IMZ}	Number (%) of ROIs		
			COX-2 (+)	dUTP (+)	MAP-2 (–)
Group 1 (n=14)	≥0.8	≥0.8	0 (0%)	0 (0%)	0 (0%)
Group 2 (n=24)	<0.8	≥0.8	4 (16.7%)	0 (0%)	0 (0%)
Group 3 (n=238)	<0.8	<0.8	79 (33.2%)	59 (24.8%)	176 (73.9%)

LNR_{IMP}, LNR for [^{125}I]IMP; LNR_{IMZ}, LNR for [^{123}I]IMZ; COX-2 (+), positive immunostaining for COX-2; dUTP (+), positive dUTP incorporation; MAP-2 (–), negative immunostaining for MAP-2

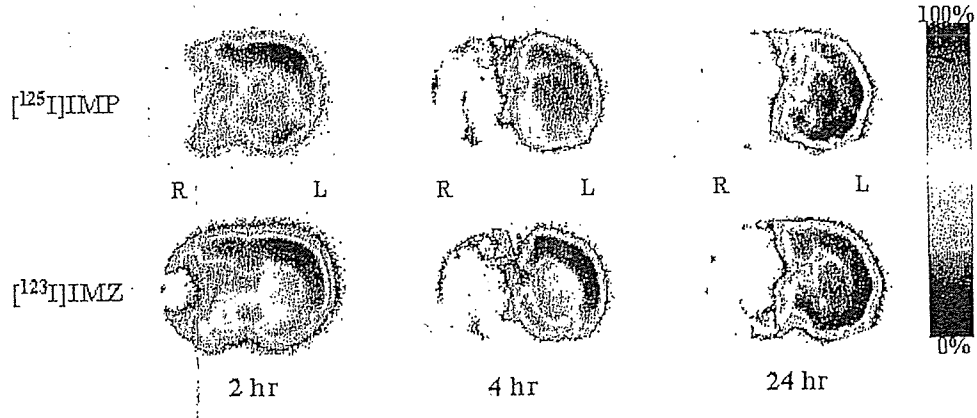

Fig. 3. Representative autoradiograms for [125I]IMP and [123I]IMZ

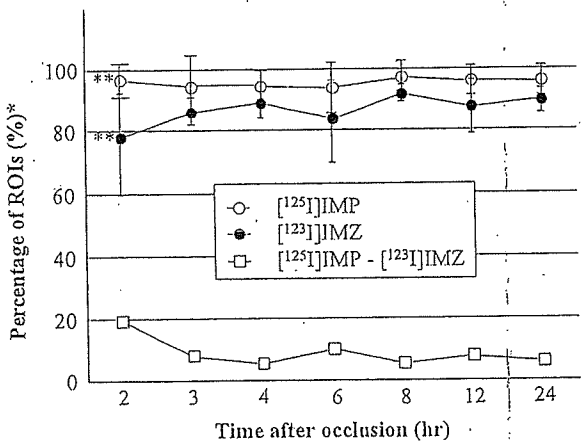

Fig. 4. Time course of the percentage of ROIs with impaired [125I]IMP or [123I]IMZ accumulation. *(Number of ROIs with LNRs less than 0.8)/(Number of total ROIs at each time point) ×100. ROIs with impaired [125I]IMP and [123I]IMZ accumulation were defined as those with LNRs less than 0.8. Significant uncoupling of accumulation between the two tracers was observed 2 h after occlusion (**P<0.01)

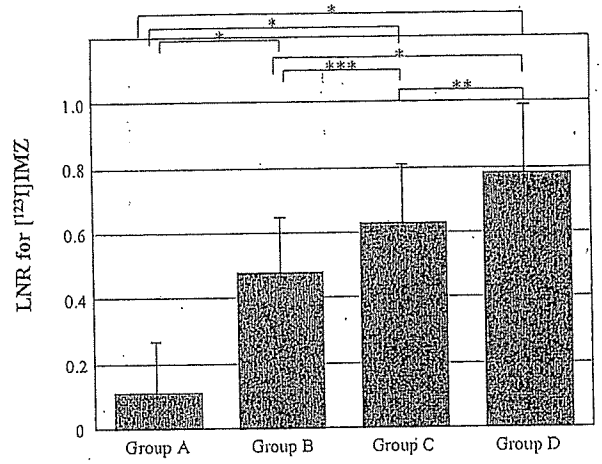

Fig. 5. The LNRs for [123I]IMZ in the four ROI groups classified on the basis of histological findings. Group A, impaired MAP-2 immunostaining; group B, preserved MAP-2 immunostaining and positive dUTP incorporation; group C, preserved MAP-2 immunostaining, negative dUTP incorporation and positive COX-2 immunostaining; group D, no histological evidence of ischaemic injury. Significant differences in LNRs between two groups: *P<0.0001, **P<0.001, ***P<0.01

decreased [123I]IMZ accumulation was smaller than that with decreased [125I]IMP accumulation (P<0.01). Uncoupling between [125I]IMP and [123I]IMZ accumulation was observed in regions surrounding the ischaemic core 2 h after occlusion, but such uncoupling reduced with time. The percentage of ROIs with impaired [123I]IMZ accumulation was significantly lower than that with decreased [125I]IMP accumulation at 2 h after occlusion (P<0.01), but not at other time points (Fig. 4).

Positivity for COX-2 was observed in 16.7% of the ROIs in the ischaemic lesions with preserved [123I]IMZ distribution (group 2) and 33.2% of the ROIs in the ischaemic lesions with decreased [123I]IMZ distribution (group 3), whereas no positivity for COX-2 was seen in non-ischaemic lesions (group 1) (Table 1). Neither positivity for dUTP incorporation nor decreased immunostaining of MAP-2 was observed in the ROIs in the lesions with preserved [123I]IMZ distribution (groups 1 and 2). Positivity for dUTP incorporation and impaired MAP-2 immunostaining were observed in 24.8% and 73.9% of the ROIs, respectively, in the lesions with decreased [123I]IMZ distribution (group 3) (Table 1).

When the ROIs were divided into four groups based on the histological findings (Fig. 5), the LNRs for [123I]IMZ in the lesions with preserved MAP-2 immunostaining (groups B, C and D) were significantly higher than those in the lesions with impaired MAP-2 immunostaining (group A; P<0.0001). The LNRs for [123I]IMZ in the lesions with preserved MAP-2 immunostaining and positive for dUTP incorporation (group B) were significantly lower than those in the lesions with preserved MAP-2 immunostaining and negative for dUTP incorporation (groups C; P<0.01, group D; P<0.0001). The LNRs for [123I]IMZ in the lesions with preserved MAP-2 immunostaining, negative for dUTP incorporation and positive for COX-2 (group C) were significantly lower

than those in the lesions with no histological evidence of an ischaemic injury (group D; $P<0.001$).

Discussion

In order to characterise [^{123}I]IMZ as a marker of neuronal viability, we compared the brain distribution of [^{123}I]IMZ with the expression of COX-2, DNA fragmentation and cellular integrity. Neither DNA fragmentation nor MAP-2 denaturation was detected in the ischaemic regions with preserved [^{123}I]IMZ accumulation. These results clearly demonstrate that neuronal DNA is still intact and cellular integrity is maintained in the ischaemic regions with preserved [^{123}I]IMZ accumulation. COX-2 expression was often observed in these regions. In addition, semiquantitative analysis based on the histological findings showed that [^{123}I]IMZ accumulation was significantly impaired in regions where DNA fragmentations were observed. Thus, [^{123}I]IMZ distribution can be an indicator that predicts the extent of neuronal damage after an ischaemic stroke.

In the present study, we compared the brain distribution of [^{123}I]IMZ with (1) CBF, (2) the expression of COX-2, a prostanoid synthesising enzyme that contributes to the progression of ischaemic damage [13, 14, 15, 16, 17], (3) fragmentation of DNA and (4) cellular integrity. The regions with preserved [^{123}I]IMZ accumulation and decreased [^{125}I]IMP accumulation, namely, uncoupling between CBF and BZR function, were observed 2 h after occlusion in regions surrounding the ischaemic core, which became smaller with time. Such uncoupling has been observed in the acute phase by several authors [9, 24, 25]. The BZR function in these regions can be regarded as intact in spite of hypoperfusion. Clinically, it was reported that the hypoperfused regions with preserved [^{123}I]IMZ accumulation do not develop infarction as determined in a follow-up evaluation with magnetic resonance imaging [3]. The uncoupling between [^{125}I]IMP and [^{123}I]IMZ accumulation may help determine the ischaemic penumbra.

Some authors [6, 10, 11] have compared [^{123}I]IMZ distribution with histological findings obtained using the haematoxylin-eosin stain. They suggested the potential of [^{123}I]IMZ for evaluating the extent of neuronal damage. The brain distribution of [^{123}I]IMZ, however, has not been correlated with the cellular response at the molecular level. The present results on the relationship between [^{123}I]IMZ accumulation and dUTP incorporation clearly demonstrate that neuronal DNA is still intact in the ischaemic regions where [^{123}I]IMZ accumulation is preserved. In addition, our results indicate the potential of [^{123}I]IMZ to significantly detect the region with DNA scission as a reduction in LNRs. It was reported that COX-2 is expressed early after an ischaemic insult and leads ischaemic neurons to apoptotic cell death [17, 26]. In the present study, COX-2 expression was often observed in the ischaemic regions with preserved [^{123}I]IMZ accumulation. COX-2 expression may precede impairment of [^{123}I]IMZ accumulation. On the other hand, the COX-2 protein was also observed in the regions where [^{123}I]IMZ accumulation decreased. The LNRs for [^{123}I]IMZ accumulation in group C (0.626±0.186) were significantly lower than those in group D (0.783±0.213). The role of the COX-2 protein may begin before the impairment of BZR function and it may continue even after this impairment, although further investigations are required to clarify this point. These results indicate that impairment of [^{123}I]IMZ accumulation may begin as early as the COX-2 expression after an acute stroke.

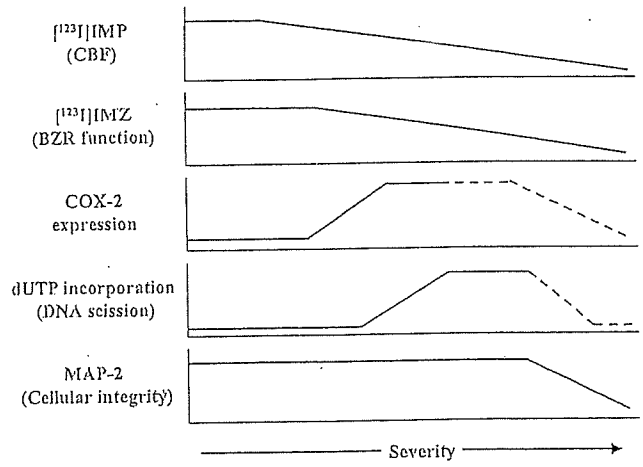

Fig. 6. Schematic representation of possible relationship between tracer accumulation and pathophysiological changes

From our results, a possible relationship between tracer accumulation and pathophysiological changes can be summarised as shown in Fig. 6. Namely, [^{125}I]IMP accumulation decreases concurrently with CBF after an ischaemic insult. COX-2 expression is often observed early after the ischaemic insult. [^{123}I]IMZ accumulation, namely, the BZR function, was impaired at a similar stage to COX-2 expression. DNA scission and impairment of cellular integrity follow the reduction in [^{123}I]IMZ accumulation.

Methodological considerations

In a clinical setting, an interval of several hours is required to sufficiently characterise BZR distribution after the [^{123}I]IMZ injection. In this study, however, rats were sacrificed 60 min after [^{123}I]IMZ administration, according to the method reported by Toyama et al. [10]. Their kinetic study indicated that specific binding of [^{123}I]IMZ can be evaluated 60 min after [^{123}I]IMZ injection in a rat model of cerebral ischaemia. Specific distribution of [^{123}I]IMZ can be achieved in a shorter period of 60 min in rats.

The relationship between tracer distribution and histological findings was evaluated simultaneously, using all samples obtained from rats sacrificed at variable time intervals after the ischaemic insult, in order to characterise [^{123}I]IMZ distribution in regions with ischaemic injury of various extent. Regional analysis in rats subjected to the same period of MCA occlusion may provide more precise information on the relationship. The relatively narrow penumbra in rats, however, may restrict such evaluation and require a higher number of rats. Thus, in the present study, the relationship was evaluated simultaneously in rats sacrificed at variable time intervals.

The average LNR for [^{123}I]IMZ in histologically normal regions was not higher than 0.8. Although, in this study, we chose 0.8 as the threshold value of the LNRs for [^{123}I]IMZ, further examinations may be needed to determine a more suitable threshold value of LNR for [^{123}I]IMZ.

In the present study, we used a dual-tracer autoradiographic technique to evaluate the blood flow and [^{123}I]IMZ binding in the same individuals. Consequently, we could not perform quantitative assessment of the blood flow and [^{123}I]IMZ binding, as it is methodologically difficult to quantitatively assess flow and IMZ binding using the dual-tracer autoradiographic technique. Further studies, especially on quantitative measurement of flow and [^{123}I]IMZ binding, are required to confirm the present results and to obtain relevant information on the flow and [^{123}I]IMZ binding in relation to the histopathological findings.

Clinical implications

The routine use of nuclear medicine for the clinical assessment of neuronal viability has been limited exclusively to the determination of CBF, oxygen and/or glucose consumption, and CBF reactivity to acetazolamide. Oxygen and glucose metabolism and CBF reactivity to acetazolamide, however, do not provide direct information on neuronal viability. Rather, these techniques yield information not only on neurons but also on astrocytes and Schwann cells. On the other hand, [^{123}I]IMZ, a central-type BZR ligand, can be a specific marker of neuronal viability. Heiss et al. suggested that imaging of BZR receptors could distinguish between irreversibly damaged and viable penumbra tissues immediately after an acute stroke using carbon-11 flumazenil and positron emission tomography [27, 28]. The present study in the rat model demonstrated that [^{123}I]IMZ can also be a marker for neuronal viability. In addition, [^{123}I]IMZ does not require in-house cyclotrons and positron emission tomography, and can be commercially supplied. The availability of this procedure is expected to favour the clinical application of [^{123}I]IMZ.

Conclusion

The present study demonstrated for the first time that impairment of [^{123}I]IMZ accumulation precedes DNA fragmentation and denaturation of cellular integrity. Our results provide the molecular basis of [^{123}I]IMZ distribution. [^{123}I]IMZ accumulation can be a clue to predicting the severity of ischaemic neuronal injury.

Acknowledgement. The authors are grateful to Professors S. Nishi, K. Miyasaka and T. Ohnishi of the Central Institute of Isotope Science, Hokkaido University, for supporting this work. We also express gratitude to Drs. T. Abumiya and K. Hikosaka for helpful discussions.

This work was supported in part by a Grant-in-Aid for Scientific Research from the Japan Society for the Promotion of Science, and Grants from Japan Heart Foundation Research, the Takeda Medical Research Foundation in Japan and the Mitubishi Pharma Research Foundation in Japan.

References

1. Garcia JH, Lassen NA, Weiller C, Sperling B, Nakagawara J. Ischemic stroke and incomplete infarction. *Stroke* 1996; 27:761–765.
2. Garcia JH, Liu KF, Ye ZR, Gutierrez JA. Incomplete infarct and delayed neuronal death after transient middle cerebral artery occlusion in rats. *Stroke* 1997; 28:2303–2310.
3. Nakagawara J, Sperling B, Lassen NA. Incomplete brain infarction of reperfused cortex may be quantitated with iomazenil. *Stroke* 1997; 28:124–132.
4. Heiss WD, Graf R, Fujita T, Ohta K, Bauer B, Lötten J, Wienhard K. Early detection of irreversibly damaged ischemic tissue by flumazenil positron emission tomography in cats. *Stroke* 1997; 28:2045–2052.
5. Heiss WD, Kracht LW, Thiel A, Grond M, Pawlik G. Penumbral probability thresholds of cortical flumazenil binding and blood flow prediction tissue outcome in patients with cerebral ischaemia. *Brain* 2001; 124:20–29.
6. Odano I, Miyashita K, Minoshima S, Nakajima T, Fujita M, Takahashi N, Ikuta F. A potential use of a ^{123}I-labeled benzodiazepine antagonist as a predictor of neuronal call viability: comparisons with ^{14}C-labeled 2-deoxyglucose autoradiography and histological examination. *Nucl Med Commun* 1996; 16:443–446.
7. Matsuda H, Tsuji S, Kuji I, Shiba K, Hisada K, Mori H. Dual-tracer autoradiography using ^{125}I-iomazenil and ^{99m}Tc-HMPAO in experimental brain ischemia. *Nucl Med Commun* 1995; 16:581–590.
8. Hatazawa J, Shimosegawa E, Satoh T, Kanno I, Uemura K. Central benzodiazepine receptor distribution after subcortical hemorrhage evaluated by means of [^{123}I]IMZ and SPECT. *Stroke* 1995; 26:2267–2271.
9. Dong Y, Fukuyama H, Nabatame H, Yamauchi H, Shibasaki H, Yonekura Y. Assessment of benzodiazepine receptors using iodine-123-labeled iomazenil single-photon emission computed tomography in patients with ischemic cerebrovascular disease. A comparison with PET study. *Stroke* 1997; 28:1776–1782.
10. Toyama H, Matsumura K, Nakashima H, Takeda K, Takeuchi A, Koga S, Yoshida T, Ichise M. Characterization of neuronal

damage by iomazenil binding and cerebral blood flow in an ischemic rat model. *Ann Nucl Med* 1998; 12:267–273.
11. Watanabe Y, Nakano T, Yutani K, Nishimura H, Kusuoka H, Nakamura H, Nishimura T. Detection of viable cortical neurons using benzodiazepine receptor imaging after reversible focal ischaemia in rats: comparison with regional cerebral blood flow. *Eur J Nucl Med* 2000; 27:308–313.
12. al-Tikriti MS, Dey HM, Zoghbi SS, Baldwin RM, Zea-Ponce Y, Innis RB. Dual-isotope autoradiographic measurement of regional blood flow and benzodiazepine receptor availability following unilateral middle cerebral artery occlusion. *Eur J Nucl Med* 1994; 21:196–202.
13. Nogawa S, Zhang F, Ross ME, Iadecola C. Cyclo-oxygenase-2 gene expression in neurons contributes to ischemic brain damage. *J Neurosci* 1997; 17:2746–2755.
14. Sairanen T, Ristimaki A, Karjalainen-Lindsberg ML, Paetau A, Kaste M, Lindsberg PJ. Cyclooxygenase-2 is induced globally in infarcted human brain. *Ann Neurol* 1998; 43:738–747.
15. Iadecola C, Forster C, Nogawa S, Clark HB, Ross ME. Cyclooxygenase-2 immunoreactivity in the human brain following cerebral ischemia. *Acta Neuropathol (Berl)* 1999; 98:9–14.
16. Hewett SJ, Uliasz TF, Vidwans AS, Hewett JA. Cyclooxygenase-2 contributes to *N*-methyl-D-asparatate-mediated neuronal cell death in primary cortical cell culture. *J Pharmacol Exp Ther* 2000; 293:417–425.
17. Takedera T, Yumoto H, Tozuka Y, Ohyashiki T. Prostaglandin E(2) induces caspase-dependent apoptosis in rat cortical cells. *Neurosci Lett* 2002; 317:61–64.
18. Gavrieli Y, Sherman Y, Ben-Sasson SA. Identification of programmed cell death in situ via specific labeling of nuclear DNA fragmentation. *J Cell Biol* 1992; 119:493–501.
19. Longa EZ, Weinstein PR, Carlson S, Cummins R. Reversible middle cerebral artery occlusion without craniotomy in rats. *Stroke* 1989; 20:84–91.
20. Minematsu K, Li L, Fisher M, Sotak CH, Davis MA, Fiandaca MS. Diffusion-weighted magnetic resonance imaging:rapid and quantitative detection of focal brain ischemia. *Neurology* 1992; 42:235–240.
21. Kuge Y, Minematsu K, Yamaguchi T, Miyake Y. Nylon monofilament for intraluminal middle cerebral artery occlusion in rats. *Stroke* 1995; 26:1655–1658.
22. Sternberger LA, Sternberger NH. The unlabeled antibody method: comparison of peroxidase- antiperoxidase with avidin-biotin complex by a new method of quantification. *J Histochem Cytochem* 1986; 34:599–605.
23. Tagaya M, Liu K, Copeland B, Seiffert D, Engler R, Garcia JH, Zoppo GJ. DNA scission after focal brain ischemia/temporal differences in two species. *Stroke* 1997; 28:1245–1254.
24. Torizuka K, Uemura K, Toru M, Shinohara Y, Nishimura T, Yonekura Y, Nakagawara J, Matsuda H, Sakai F, Matsuda K, Fukuyama H, Morimoto K. A phase 3 clinical trial of ^{123}I-iomazenil, a new central-type benzodiazepine receptor imaging agent. Part 4. Report on clinical usefulness in diagnosis of cerebrovascular diseases. *Kaku Igaku* 1996; 33:329–344.
25. Moriwaki H, Matsumoto M, Hashikawa K, Oku N, Ishida M, Seike Y, Fukuchi K, Hori M, Nishimura T. Iodine-123-iomazenil and iodine-123-iodoamphetamine SPECT in major cerebral artery occlusive disease. *J Nucl Med* 1998; 39:1348–1353.
26. Matsuoka Y, Okazaki M, Zhao H, Asai S, Ishikawa K, Kitamura Y. Phosphorylation of c-Jun and its localization with heme oxygenase-1 and cyclooxygenase-2 in CA1 pyramidal neurons after transient forebrain ischemia. *J Cereb Blood Flow Metab* 1999; 19:1247–1255.
27. Heiss WD, Grond M, Thiel A, Ghaemi M, Sobesky J, Bauer B, Wienhard K. Permanent cortical damage detected by flumazenil positron emission tomography in acute stroke. *Stroke* 1998; 29:454–461.
28. Heiss WD, Kracht L, Grond M, Rudolf J, Bauer B, Wienhard K, Pawlik G. Early [^{11}C]flumazenil/H_2O positron emission tomography predicts irreversible ischemic cortical damage in stroke patients receiving acute thrombolytic therapy. *Stroke* 2000; 31:366–369.

Original Article

Association of Genetic Polymorphisms of Sodium-Calcium Exchanger 1 Gene, *NCX1*, with Hypertension in a Japanese General Population

Yoshihiro KOKUBO[*1], Nozomu INAMOTO[*1], Hitonobu TOMOIKE[*1], Kei KAMIDE[*2], Shin TAKIUCHI[*2], Yuhei KAWANO[*2], Chihiro TANAKA[*3], Yuki KATANOSAKA[*3], Shigeo WAKABAYASHI[*3], Munekazu SHIGEKAWA[*3], Otosaburo HISHIKAWA[*4], and Toshiyuki MIYATA[*3]

The Na^+/Ca^{2+} exchanger (NCX) is a membrane protein involved in calcium homeostasis, catalyzing the exchange of one Ca^{2+} ion for three Na^+ ions across the cell membrane. The Na^+/Ca^{2+} exchange has been suggested to play a role in the pathogenesis of hypertension. Therefore, we examined whether genetic variations in *NCX1* were associated with hypertension. Among 15 polymorphisms identified in 96 hypertensive subjects by sequencing the entire exon and promoter regions of *NCX1*, 7 representative polymorphisms with a minor allele frequency of greater than 4% were genotyped in 1,865 individuals, of whom 787 were hypertensive and 1,072 were normotensive. These subjects were residents of Suita City and were randomly selected as a population for the Suita cohort study. Multivariate logistic regression analysis performed after adjusting for age, body mass index, hyperlipidemia, diabetes mellitus, smoking, and drinking revealed that the −23200T>C and −23181T>C polymorphisms in the 5′ upstream region of exon 1c were significantly associated with hypertension in men (−23200T>C: CC *vs.* TC+TT: odds ratio=0.61; 95% confidence intervals: 0.39 to 0.97; $p=0.04$) and in women (−23181T>C: CC *vs.* TC+TT: odds ratio=1.45; 95% confidence intervals: 1.04 to 2.02; $p=0.03$), respectively. Thus, our study suggests that *NCX1* is one of the genes related to susceptibility to essential hypertension in the Japanese general population.

(*Hypertens Res* 2004; 27: 697–702)

***Key Words*: NCX1, Na^+/Ca^{2+} exchanger, gene variants, hypertension**

Introduction

The Na^+/Ca^{2+} exchanger (NCX) is an important membrane protein involved in calcium homeostasis in various cell types and catalyzes the electrogenic exchange of one Ca^{2+} ion for three Na^+ ions across the plasma membrane (*1–3*). The Na^+/Ca^{2+} exchange has been well demonstrated to play a role in the pathogenesis of hypertension. Blaustein *et al.* suggested that excessive Na^+ retention may secrete an ouabain-like substance that increases the cytosolic Na^+ concentration by inhibiting the plasmalemmal Na^+-pump, which increases the cytosolic Ca^{2+} concentration ($[Ca^{2+}]_i$) by reducing Ca^{2+}-extrusion *via* Na^+/Ca^{2+} exchange (*4–6*). The increase in arteri-

From the [*1]Division of Preventive Cardiology, [*2]Division of Hypertension and Nephrology, and [*3]Research Institute, National Cardiovascular Center, Suita, Japan, and [*4]Suita City Medical Association, Suita, Japan.

This study was supported by the Program for Promotion of Fundamental Studies in Health Science of the Pharmaceuticals and Medical Devices Agency (PMDA) of Japan MPJ-3.

Address for Reprints: Yoshihiro Kokubo, M.D., Ph.D., Division of Preventive Cardiology, National Cardiovascular Center, 5–7–1 Fujishiro-dai, Suita 565–8565, Japan. E-mail: ykokubo@hsp.ncvc.go.jp

Received March 2, 2004; Accepted in revised form June 4, 2004.

Table 1. Basic Characteristics of Subjects in Suita, a Japanese Urban Population, 2002

	Men (n=858)	Women (n=1,007)
Age (year)	66.3±11.1*	63.3±11.0*
Systolic blood pressure (mmHg)	131.9±19.5*	128.0±19.6*
Diastolic blood pressure (mmHg)	79.7±10.7*	76.6±10.7*
Body mass index (kg/m^2)	23.3±3.0*	22.3±3.2*
Total cholesterol (mmol/l)	5.10±0.78	5.57±0.79*
HDL-cholesterol (mmol/l)	1.42±0.36	1.67±0.40*
Current smokers (%)	30.1†	6.3†
Current drinkers (%)	67.0†	29.3†
Present illness (%)		
Hypertension	47.4†	38.2
Hyperlipidemia	27.4	55.2†
Diabetes mellitus	12.6†	5.2

Values are mean±SD or percentage. Hypertension indicates systolic blood pressure ≥140 mmHg and/or diastolic blood pressure ≥90 mmHg or antihypertensive medication; hyperlipidemia, total cholesterol ≥5.68 mmol/l (220 mg/dl) or antihyperlipidemia medication; diabetes, fasting plasma glucose ≥7.0 mmol/l (126 mg/dl) or non-fasting plasma glucose ≥11.1 mmol/l (200 mg/dl) or HbA1c ≥6.5% or antidiabetic medication. * $p<0.05$ between women and men by Student's t-test. † $p<0.05$ between women and men by χ^2 test. HDL, high-density lipoprotein.

al tone caused by high $[Ca^{2+}]_i$ would thus result in an elevation of blood pressure. Indeed, several previous studies have reported that Na^+/Ca^{2+} exchange activity was altered in the renal arterioles or arterial smooth muscle of spontaneous or salt-sensitive hypertensive rats (*7–11*). However, it is unknown whether such a mechanism relates to the occurrence of essential hypertension.

Of three isoforms (NCX1–3) derived from different genes, NCX1 is predominantly expressed in the heart, neurons and renal tubules, but is expressed at lower levels in other tissues, including the smooth muscle, skeletal muscle, lung and spleen (*1–3*). The *NCX1* gene (*SLC8A1*) is located on human chromosome 2p22.1 and includes 12 exons (*12*). There are at least 12 splice variants generated in different combinations from six exons in a tissue-specific manner (*13*). In addition, five exons encode 5′-untranslated sequences that are under the control of three tissue-specific promoters (*14–17*).

This study was undertaken to identify genetic variations in *NCX1* in a group of hypertensive subjects, and to examine the association of these variations with the presence of hypertension in a general population. In contrast to other association studies, which often focus on a limited number of polymorphisms in a gene, our study evaluated the full array of coding- and promoter-sequence polymorphisms in *NCX1*.

Methods

Subjects of the Suita Population Study

The subjects of the Suita study consisted of 14,200 men and women (30 to 79 years of age), who had been randomly selected from the municipal population registry and stratified by in consideration of gender and age (stratified in 10-year intervals). They were all invited, by letter, to receive medical and behavioral examinations every 2 years at the Division of Preventive Cardiology, National Cardiovascular Center, Japan. DNA from the leukocytes was collected from participants who visited the National Cardiovascular Center between May 2002 and February 2003. All of the participants were Japanese. Only those who gave written informed consent for genetic analyses were included in this study. The study protocol was approved by the Ethical Review Committee of the National Cardiovascular Center. In this study, the genotypes of 1,865 samples were determined. The characteristics of 1,865 participants (858 men, 1,007 women) are shown in Table 1. Routine blood examinations that included total serum cholesterol, high-density lipoprotein (HDL) cholesterol, triglyceride, and glucose levels were performed. A physician or nurse interviewed each patient in regard to smoking and drinking habits and personal history of cardiovascular disease, including angina pectoris, myocardial infarction, and/or stroke.

Blood pressure was measured in a sitting position after at least 10 min of rest. Systolic and diastolic blood pressures (SBP/DBP) were taken as the means of two measurements recorded more than 3 min apart by well-trained doctors. Hypertension was defined as SBP of ≥140 mmHg, DBP of ≥90 mmHg, or the current use of antihypertensive medication (*18*). Diabetes mellitus was defined as fasting plasma glucose ≥7.0 mmol/l (126 mg/dl), non-fasting plasma glucose ≥11.1 mmol/l (200 mg/dl), current use of antidiabetic medication, or HbA1c ≥6.5%. Hyperlipidemia was defined as total cholesterol ≥5.68 mmol/l (220 mg/dl) or current use of antihyperlipidemia medication. Body mass index (BMI)

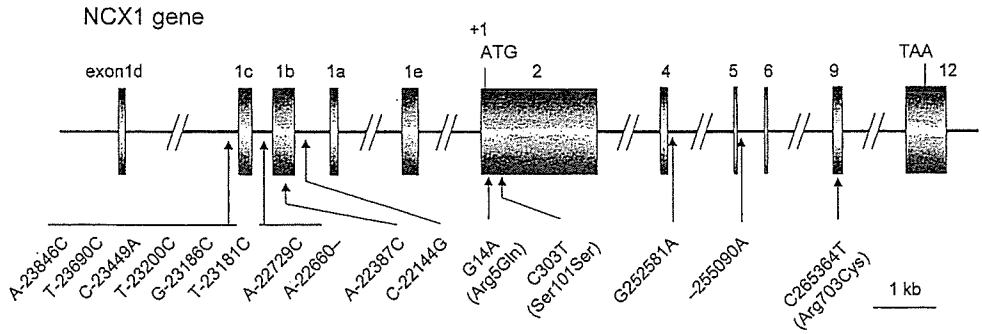

Fig. 1. *Genome structure of human* NCX1. *The* NCX1 *gene consists of sixteen exons, five (exons 1a–1e) of which direct tissue-specific transcription and eleven (exons 2–12) of which encode the open reading frame (17). The five tissue-specific transcription exons (exons 1a–1e) and the exons in which the SNPs were identified are depicted. The nucleotide changes and amino acid substitutions are also shown. The A of the ATG of the initiator Met codon is denoted nucleotide +1.*

was calculated as weight (in kg) divided by height (in m) squared.

Direct Sequencing for Single Nucleotide Polymorphism (SNP) Discovery and Genotyping of Polymorphisms

For DNA sequencing, 96 patients with essential hypertension were recruited from the Division of Hypertension and Nephrology, National Cardiovascular Center, Japan. The method of direct sequencing was described previously (*19*). Fifteen polymorphisms were identified by sequencing and 7 representative polymorphisms with a minor allele frequency of greater than 4% were genotyped by the TaqMan-polymerase chain reaction (PCR) system (*20*). Only those who gave written informed consent for genetic analyses were included in this study. The study protocol was approved by the Ethical Review Committee of the National Cardiovascular Center.

Statistical Analysis

Analysis of variance was used to compare mean values between groups, and if overall significance was demonstrated, the intergroup difference was assessed by means of a general linear model. Frequencies were compared by χ^2 analysis.

Logistic regression analyses were used to examine the association between the genotypes and blood pressure in each sex with consideration for potential confounding risk variables, including age, BMI, present illness (hyperlipidemia and diabetes mellitus), lifestyle (smoking and drinking), and antihypertensive medication. For multivariate risk predictors, the adjusted odds ratios were given with 95% confidence intervals. The relationship between genotype and risk of hypertension was expressed in terms of the odds ratios adjusted for possible confounding effects including age, BMI, present illness (hyperlipidemia and diabetes mellitus), and lifestyle (smoking and drinking). SAS statistical software (release 8.2; SAS Institute, Cary, USA) was used for statistical analyses (*21*).

Results

Basic Characteristics of Subjects in the Suita Study

The characteristics of the 1,865 participants (858 men, 1,007 women) are summarized in Table 1. Age, SBP, DBP, BMI, percentage of current smokers, percentage of current drinkers, and prevalence of hypertension and diabetes mellitus were significantly higher in men than in women. Total cholesterol, HDL-cholesterol, and percentage of hyperlipidemia were significantly higher in women than in men.

Polymorphisms of *NCX1*

The *NCX1* gene has a complicated genome structure containing five alternative 5′ exons producing separate tissue-specific promoters and six exons encoding open reading frames (Fig. 1). We sequenced the entire exon and promoter regions of *NCX1* from 96 patients (182 alleles) with hypertension, and identified 15 polymorphisms (Table 2, Fig. 1). We identified two missense mutations, Arg5Gln in exon 2 and Arg703Cys in exon 9, in *NCX1* (Table 2). Each of the missense mutations was identified in one out of 96 individuals, indicating that their allele frequencies were rare. Two SNPs, −23200T>C and −23186G>C, were in linkage disequilibrium. Seven representative polymorphisms with a minor allele frequency of greater than 4% were genotyped for the association study.

Susceptible SNPs Related to Hypertension

Seven polymorphisms in *NCX1* were genotyped in 1,865 individuals, of whom 787 were hypertensive and 1,072 were normotensive. The primers and probes of the TagMan-PCR system and the genotyping results are summarized in Table

Table 2. List of 15 Polymorphisms and Their Allele Frequencies in the *NCX1* Gene Identified by Direct Sequencing

Allele 1/Allele 2 SNPs	TaqMan typing	Amino acid change	Region	Allele 1 Homo	Hetero	Allele 2 Homo	Total	Allele frequency Allele 1	Allele frequency Allele 2	Flanking sequence
−23846A>C			intron 1d	94	1	0	95	0.995	0.005	tcacactgcctt[a/c]aattcagggact
−23690T>C	typing		intron 1d	62	31	2	95	0.816	0.184	aaatttaactta[t/c]agcaaggaaaga
−23449C>A	typing		intron 1d	85	9	1	95	0.942	0.058	catactcacatt[c/a]atgtttgaggag
−23200T>C*	typing		intron 1d	0	9	86	95	0.047	0.953	attccgcccccct[t/c]tttgttgcggag
−23186G>C*			intron 1d	0	9	86	95	0.047	0.953	ttgttgcggagg[g/c]aaactgaggttc
−23181T>C	typing		intron 1d	18	57	20	95	0.489	0.511	gcggaggcaaac[t/c]gaggttcctgga
−22729A>C	typing		intron 1c	71	23	1	95	0.868	0.132	taattatgagga[a/c]agtgatttattg
−22660delA			intron 1c	94	1	0	95	0.995	0.005	gattgctgcatt[a/−]ggtttttccca
−22387A>C		5′ UTR	exon 1b	93	3	0	96	0.984	0.016	attaaaaaaaaa[a/c]tcattgatatat
−22144C>G	typing		intron 1b	84	9	2	95	0.932	0.068	gcgcggccacaa[c/g]gcactgcgggggc
14G>A		Arg5Gln	exon 2	95	1	0	96	0.995	0.005	tgtacaacatgc[g/a]gcgattaagtct
303C>T		Ser101Ser	exon 2	95	1	0	96	0.995	0.005	tcggttcatgtc[c/t]tctatagaagtc
252581G>A	typing		intron 4	45	40	11	96	0.677	0.323	tcttctctctcc[g/a]tgtctccctact
255089–255090insA			intron 5	94	1	0	95	0.995	0.005	tcaggtgataca[−/a]gtagctctgtga
265364C>T		Arg703Cys	exon 9	95	1	0	96	0.995	0.005	gcagaaatgggg[c/t]gccccatcctgg

The A of the ATG of the initiator Met codon is denoted nucleotide +1. * The apparent linkage disequilibrium ($r^2 \geq 0.5$). NCX1, Na^+/Ca^{2+} exchanger; SNP, single nucleotide polymorphism.

3. Multivariate logistic regression analysis after adjusting for confounding risk variables such as age, BMI, hyperlipidemia, diabetes mellitus, smoking, and drinking, revealed that two polymorphisms, −23200T>C and −23181T>C, in the 5′ upstream region of exon 1c were significantly associated with hypertension in men (−23200T>C: CC *vs.* TC+TT: odds ratio=0.61; 95% confidence interval: 0.39 to 0.97; $p=0.04$) and in women (−23181T>C: CC *vs.* TC+TT: odds ratio=1.45; 95% confidence interval: 1.04 to 2.02; $p=0.03$), respectively (Table 4). When normotension was defined as SBP ≤120 mmHg, DBP ≤80 mmHg, and the absence of anti-hypertensive medication, and hypertension was defined as SBP ≥160 mmHg, DBP ≥100 mmHg, or the current use of antihypertensive medication, −23200T>C polymorphism was significantly associated with hypertension in men (CC *vs.* TC+TT: odds ratio=0.42; 95% confidence interval: 0.20 to 0.92; $p=0.03$) after adjusting for the confounding factors described above.

Discussion

In this study, we sequenced the exon and promoter regions of *NCX1* and identified 15 polymorphisms. Seven representative polymorphisms were genotyped from 1,865 subjects to examine the association of hypertension with *NCX1*. After adjustment for various confounding factors, we identified that the −23200T>C polymorphism in the 5′ upstream region of exon 1c was significantly associated with hypertension in men and the −23181T>C polymorphism in the 5′ upstream region of exon 1c was significantly associated with hypertension in women.

The *NCX1* gene has at least 12 splice variants generated in different combinations from six exons in a tissue-specific manner (*13*). In addition, three exons encode 5′-untranslated sequences that are under the control of three tissue-specific promoters (*14–16*). Exon 1c is a part of the "heart" specific transcript (*17*) and its upstream region is not likely a promoter. Therefore, the −23200T>C and −23181T>C polymorphisms present in the upstream region of exon 1c are not likely to be directly involved in transcription of *NCX1*. Rather, these polymorphisms may be in linkage disequilibrium with other polymorphisms in the region that were not examined by sequencing in this study.

In this study, the −23200T>C polymorphism in men and −23181T>C polymorphism in women were identified as SNPs conferring susceptibility for hypertension. It is well known that the greater incidence of hypertension and coronary artery disease in men is, in part, related to gender differences in possible vascular protective effects of the female sex hormones estrogen and progesterone. Furthermore, NCX1 might be related to salt-sensitive hypertension (*22*). Since there is a gender difference in salt-sensitivity and plasma renin activity (*23*, *24*), −23200T>C and −23181T>C in *NCX1* may be linked with unidentified causative genetic variations that would be influenced by the female sex hormones and/or salt-sensitivity.

In this study, we identified two missense mutations, Arg5Gln in exon 2 and Arg703Cys in exon 9, in *NCX1*. Arg5 is located within the signal peptide sequence consisting of the first N-terminal 35 amino acids of NCX1, which are removed during biosynthesis (*1*). We expressed a mutant canine NCX1 with the Arg5Gln substitution in the fibroblastic

Table 3. Genotyping Conditions and Results of *NCX1* Polymorphisms in 1,818 Individuals by TaqMan-PCR Method

SNP	Primer	Probe	Genotypes results
−23690T>C	CTCTCCCCACAGGTCATTCTG	Fam-ATTTAACTTATAGCAAGGAA-MGB	(TT/TC/CC)
	GCAGGAATCGTTCTTGCCTAA	Vic-TTAACTTACAGCAAGGAA-MGB	=(1,140/590/88)
−23449C>A	GAATCTGCAATCCCCATGTGAT	Fam-CTCACATTCATGTTTGAG-MGB	(CC/CA/AA)
	AGAACCACTGCTCTAGGCCAAT	Vic-ACTCACATTAATGTTTGAGG-MGB	=(1,542/261/15)
−23200T>C	TTCTGAGGTGCAAGGAGGGTT	Fam-CCCCCTTTTTGTTGC-MGB	(TT/TC/CC)
	GGCAGTCACCACGACTGATAGA	Vic-CCCCCTCTTTGTTG-MGB	=(4/196/1,618)
−23181T>C	GGCAGTCACCACGACTGATAGA	Fam-TCCAGGAACCTCAGTTT-MGB	(TT/TC/CC)
	AGGCTATTTCTTCCATTCCGC	Vic-CCAGGAACCTCGGTTT-MGB	=(503/869/446)
−22729A>C	GCCTGGTGCAGTGTTCCTTTA	Fam-ATTATGAGGAAAGTGATTTA-MGB	(AA/AC/CC)
	GCCCTTTCCAAGAGAAGCATTA	Vic-TATGAGGACAGTGATTTA-MGB	=(1,369/406/43)
−22144C>G	AAAAGAAAAGTTGCAGCGCCT	Fam-CCACAACGCACTGC-MGB	(CC/CG/GG)
	TTTTTCGATTTCCTGCCGG	Vic-CACAAGGCACTGCG-MGB	=(1,687/131/0)
252581G>A	AAACAAAGACATACCAGCGAGAAA	Fam-CTCTCTCCGTGTCTC-MGB	(GG/GA/AA)
	AAATTGCTAAAGCTTCAAAGGCA	Vic-TCTCTCCATGTCTCC-MGB	=(823/798/197)

PCR, polymerase chain reaction; SNP, single nucleotide polymorphism.

Table 4. Odds Ratio of −23200T>C Polymorphism in Men and −23181T>C Polymorphism in Women*

Gender	SNP	OR (95% CI)		*p*	OR (95% CI)		*p*
Men	−23200T>C	CC	1 (reference)		CC+TC	1 (reference)	
		TC+TT	0.61 (0.39–0.97)	0.04	TT	—	—
Women	−23181T>C	CC	1 (reference)		CC+TC	1 (reference)	
		TC+TT	1.45 (1.04–2.02)	0.03	TT	1.39 (1.00–1.92)	0.05

*Conditional logistic analysis, adjusted for age, body mass index, present illness (hyperlipidemia and diabetes mellitus), and lifestyle (smoking and drinking). SNP, single nucleotide polymorphism; OR, odds ratio; CI, confidence intervals.

cell line CCL39, and found that this mutant NCX1 was properly targeted into the plasma membrane and exhibited the normal Na^+/Ca^{2+} exchange activity (unpublished observations), consistent with previous reports stating that signal sequence is not essential for functional expression of the NCX1 protein (*25*, *26*). On the other hand, Arg703 is located within the large cytoplasmic loop connecting the transmembrane segments 5 and 6, which are not essential for the functional expression of the NCX1 protein (*1*). Thus, the two rare mutations identified in this study would not grossly impair the function of NCX1.

In summary, we showed that the SNPs −23200T>C and −23181T>C in *NCX1* were associated with hypertension. The pathophysiological functional behaviors of these polymorphisms remain to be clarified. In future studies, it will be necessary to clarify the function of these polymorphisms or to identify the causative polymorphisms that are in linkage disequilibrium with these polymorphisms.

Acknowledgements

We would like to express our highest gratitude to Dr. Soichiro Kitamura, President of the National Cardiovascular Center, for his support of the Millennium genome project (MPJ-3). We would also like to thank Dr. Katsuyuki Kawanishi, Dr. Toshifumi Mannami, and Mr. Tadashi Fujikawa for their continuous support of our population survey in Suita City. We also thank the members of the Satsuki-Junyukai. We also thank all the staff in the Division of Preventive Cardiology for supporting medical examination and M. Banno, Y. Tokunaga, and C. Imai for their technical assistance. Finally, we are grateful to Dr. Tetsuji Yokoyama for his statistical advice.

References

1. Philipson KD, Nicoll DA: Sodium-calcium exchange: a molecular perspective. *Annu Rev Physiol* 2000; **62**: 111–133.
2. Shigekawa M, Iwamoto T: Cardiac Na^+-Ca^{2+} exchange: molecular and pharmacological aspects. *Circ Res* 2001; **88**: 864–876.
3. Blaustein MP, Lederer WJ: Sodium/calcium exchange: its physiological implications. *Physiol Rev* 1999; **79**: 763–854.
4. Blaustein MP: Sodium ions, calcium ions, blood pressure regulation, and hypertension: a reassessment and a hypothesis. *Am J Physiol* 1977; **232**: C165–C173.
5. Blaustein MP: Physiological effects of endogenous ouabain: control of intracellular Ca^{2+} stores and cell respon-